LEVEL II

(14) AFWAL-TR-81-1017

(6) STUDY AND CHARACTERIZATION OF TM$_{010}$ (Sub) CYLINDRICAL RESONANT CAVITY COMBINERS

(10) Donald L. Allen, First Lieutenant, USAF
Microwave Technology Branch
Electronic Technology Division



(11) April 1981

(12) 86

TECHNICAL REPORT AFWAL-TR-81-1017

(9) Final Report, [redacted] Jan [redacted]-Dec [redacted]80)



(16) 2002

(17) 02

Approved for public release; distribution unlimited



62204F

AVIONICS LABORATORY
AIR FORCE WRIGHT AERONAUTICAL LABORATORIES
AIR FORCE SYSTEMS COMMAND
WRIGHT-PATTERSON AIR FORCE BASE, OHIO 45433

*NOTICE*

*When Government drawings, specifications, or other data are used for any purpose other than in connection with a definitely related Government procurement operation, the United States Government thereby incurs no responsibility nor any obligation whatsoever; and the fact that the government may have formulated, furnished, or in any way supplied the said drawings, specifications, or other data, is not to be regarded by implication or otherwise as in any manner licensing the holder or any other person or corporation, or conveying any rights or permission to manufacture use, or sell any patented invention that may in any way be related thereto.*

*This report has been reviewed by the Office of Public Affairs (ASD/PA) and is releasable to the National Technical Information Service (NTIS). At NTIS, it will be available to the general public, including foreign nations.*

*This technical report has been reviewed and is approved for publication.*

Donald L. Allen

DONALD L. ALLEN, 1Lt
Microwave Techniques & Appl. Group
Electronic Technology Division
Avionics Laboratory

Alan R. Mertz

ALAN R. MERTZ, Capt, USAF
Ch, Microwave Tech & Appl. Gp
Electronic Technology Division
Avionics Laboratory

*FOR THE COMMANDER*

Donald S. Rees

DONALD S. REES, Chief
Microwave Technology Branch
Avionics Laboratory

*"If your address has changed, if you wish to be removed from our mailing list, or if the addressee is no longer employed by your organization please notify* AFWAL/AADM, *W-PAFB, OH 45433 to help us maintain a current mailing list".*

*Copies of this report should not be returned unless return is required by security considerations, contractual obligations, or notice on a specific document.*

SECURITY CLASSIFICATION OF THIS PAGE (When Data Entered)

| REPORT DOCUMENTATION PAGE | READ INSTRUCTIONS BEFORE COMPLETING FORM |
|---|---|
| 1. REPORT NUMBER: AFWAL-TR-81-1017 | 2. GOVT ACCESSION NO.: AD-A100 491 |
| 3. RECIPIENT'S CATALOG NUMBER: | |
| 4. TITLE (and Subtitle): Study and Characterization of $TM_{ono}$ Cylindrical Resonant Cavity Combiners | 5. TYPE OF REPORT & PERIOD COVERED: Final, Jan-Dec 1980 |
| | 6. PERFORMING ORG. REPORT NUMBER: |
| 7. AUTHOR(s): Donald L. Allen | 8. CONTRACT OR GRANT NUMBER(s): |
| 9. PERFORMING ORGANIZATION NAME AND ADDRESS: Microwave Technology Branch, AFWAL/AADM<br>Avionics Laboratory<br>Air Force Wright Aeronautical Laboratories, WPAFB, OH 45433 | 10. PROGRAM ELEMENT, PROJECT, TASK AREA & WORK UNIT NUMBERS: 20020247 |
| 11. CONTROLLING OFFICE NAME AND ADDRESS: Avionics Laboratory (AFWAL/AADM-2)<br>Air Force Wright Aeronautical Labs<br>Wright-Patterson AFB, Ohio 45433 | 12. REPORT DATE: December 1980<br>13. NUMBER OF PAGES: 77 |
| 14. MONITORING AGENCY NAME & ADDRESS (if different from Controlling Office): Same | 15. SECURITY CLASS. (of this report): Unclassified<br>15a. DECLASSIFICATION/DOWNGRADING SCHEDULE |
| 16. DISTRIBUTION STATEMENT (of this Report): Approved for public release; distribution unlimited. | |
| 17. DISTRIBUTION STATEMENT (of the abstract entered in Block 20, if different from Report) | |
| 18. SUPPLEMENTARY NOTES | |
| 19. KEY WORDS (Continue on reverse side if necessary and identify by block number):<br>Power Combining<br>Circular Cylindrical Resonant Cavities<br>Diode Combiner Characterization<br>Microwave Circuit Analysis | |
| 20. ABSTRACT (Continue on reverse side if necessary and identify by block number): In this investigation the $TM_{ono}$ cylindrical resonant cavity combiner is studied and characterized with the objective of improving the understanding of the design parameters of this microwave circuit. The study portion of the investigation involves presenting the fundamental theory of the cylindrical resonant cavity and coaxial diode circuits which make up a cylindrical resonant cavity combiner, the general modelling of two-port resonant cavities, and the equivalent circuit impedance relations of the Kurokawa combiner | |

DD FORM 1 JAN 73 1473 EDITION OF 1 NOV 65 IS OBSOLETE

SECURITY CLASSIFICATION OF THIS PAGE (When Data Entered)

model [2] which has been widely used by researchers in this area. The objective of using this model was to examine its applicability to higher-order $TM_{0n0}$ mode combiners. The characterization section includes the passive two-port measurement of impedance and transmission coefficient on a TM020 test combiner under various circuit conditions. A correlation between the measured and calculated impedance at a single coaxial line is presented and the results demonstrate that the Kurokawa model generally replicates the measured response. However, it is shown that there exists a relationship between the coupling coefficient at the cavity/coaxial line interface and the number of coaxial lines which must be included in the Kurokawa model. The results of the transmission measurements indicate that to achieve maximum combining efficiency, a high unloaded cavity Q must be maintained (i.e. through the use of small coaxial lines) and that the microwave absorber characteristic impedance must be minimized without causing instability in operation with IMPATT diodes.

# PREFACE

I would like to take this opportunity to express my deepest appreciation to those persons who either directly or indirectly supported this project. Thanks go to Dr. Bernard Schmidt, my advisor, for his invaluable assistance and to professors Adrian Morgan and Reinhold Kubach for their assistance in evaluating this thesis. I would also like to acknowledge and say thank you to Mr. Rudy Mastroianni of Norden Systems, Inc. for his helpful comments on the theory of resonant combiners and to the Microwave Technology Branch of the Avionics Laboratory at Wright-Patterson AFB for their support and use of their facilities.

TABLE OF CONTENTS

CHAPTER

I. INTRODUCTION.....1

Statement of the Problem

II. CYLINDRICAL RESONANT CAVITY COMBINER THEORY.....3

General Characteristics
The Cylindrical Resonant Cavity
Coaxial Diode Circuits

III. CYLINDRICAL RESONANT CAVITY COMBINER MODELLING.....15

General Modelling of Two-Port Resonant Cavities
$TM_{ono}$ Combiner Equivalent Circuit Impedance Relations

IV. $TM_{020}$ TEST COMBINER CHARACTERIZATION.....29

$TM_{020}$ Test Combiner Description
$TM_{020}$ Test Combiner Measurements
Correlation of Measured and Calculated Results

V. SUMMARY AND CONCLUSIONS.....65

APPENDIX

A. ZCOMB Program.....68

B. IN Z Program.....74

REFERENCES.....76

## LIST OF FIGURES


1. Cross Section of a $TM_{ono}$ Cylindrical Resonant Cavity Combiner...4
2. $TM_{ono}$ Mode Field Configurations.....7
3. $TM_{mno}$ Mode Field Configurations.....7
4. Relative Separation Between Various $TM_{mno}$ Modes.....10
5. Various Microwave Absorber Load Geometries.....14
6. Equivalent Circuit of a General Lossless Two-Port Resonant Cavity.....18
7. Single-Mode Resonant Cavity Equivalent Circuit.....20
8. Equivalent Circuit of a $TM_{ono}$ Combiner with N Coaxial Lines.....24
9. $TM_{020}$ Test Combiner Cross Section.....30
10. HP 8545A Automatic Network Analyzer System.....32
11. Graphical Method for Measuring Q.....35
12. $TM_{ono}$ Combiner Equivalent Circuit with Coaxial Lines Removed...36
13. $TM_{020}$ Test Combiner Input Impedance, d=.150".....38
14. $TM_{020}$ Test Combiner Input Impedance, d=.300".....39
15. Microwave Absorber Load Test Circuit.....42
16. Microwave Absorber Measured versus Calculated Load Impedance...43
17. Coaxial Line Impedance, one line present, 50 ohm input, d=.150".....46
18. Coaxial Line Impedance, four lines present, 50 ohm input, d=.150".....47
19. Coaxial Line Impedance, one line present, 50 ohm input, d=.300".....48
20. Coaxial Line Impedance, four lines present, 50 ohm input, d=.300".....49
21. Equivalent Circuit of a $TM_{ono}$ Combiner with the Cavity Probe Short Circuited and One Coaxial Line Present.....51
22. Coaxial Line Impedance, one line present, input shorted, d=.150".....53

LIST OF FIGURES(con't)


23. Coaxial Line Impedance, four lines present, input shorted, d=.150"....54

24. Coaxial Line Impedance, one line present, input shorted, d=.300"....55

25. Coaxial Line Impedance, four lines present, input shorted, d=.300"....56

26. Center Probe to Coaxial Line Transmission, d=.150"....58

27. Center Probe to Coaxial Line Transmission, d=.300"....58

28. Coaxial Line-to-Line Isolation, input shorted, d=.300"....60

29. Coaxial Line-to-Line Isolation, 50 ohm input, d=.300"....60

30. Calculated Coaxial Line Impedance Response, one coaxial line, d=.300", $n_2^2=6.5 \times 10^{-4}$....63

31. Calculated Coaxial Line Impedance Response, four lines present, d=.300", $n_2^2=.406 \times 10^{-4}$....64

32. Flowchart of ZCOMB Program....69

## LIST OF TABLES

1. Ordered Zeroes $\chi_{mn}$ of $J_m(\chi_{mn})$.....8

2. Ordered Zeores $\chi'_{mn}$ of $J'_m(\chi'_{mn})$.....8

3. $TM_{020}$ Cavity Test Combiner Measured versus Calculated Q's.....33

4. ZCOMB Program Listing.....71

5. ZCOMB Program Register Listing.....73

6. IN 2 Program Listing.....75

# CHAPTER I

## INTRODUCTION

The objective of this investigation has been to study and characterize the $TM_{ono}$ cylindrical resonant cavity combiner with emphasis on improving the understanding of the passive design parameters of this microwave circuit. Since 1971, the $TM_{ono}$ cylindrical resonant cavity combiner has been widely used as a microwave and millimeter wave circuit structure for combining the individual RF outputs of Impact-Ionization-Avalanche-Transit-Time (IMPATT) diodes. Harp and Stover [1] first demonstrated the use of a $TM_{ono}$ cylindrical resonant cavity to combine the outputs of several IMPATT diodes situated in coaxial circuits [2] located at the periphery of a $TM_{ono}$ cavity. Subsequently in recent years, several power combiner designs [5-7] have successfully employed this type of circuit in combining from 4 to 64 IMPATT diodes. The cylindrical resonant cavity combiner design has been successful because it offers many advantages such as high combining efficiency, a large capacity for combining IMPATT diodes, mechanical and electrical frequency tuning, equal amplitude and phase distribution to each diode circuit, large RF power generation per unit volume, and ease of fabrication.

## Statement of the Problem

Even though the $TM_{ono}$ cylindrical resonant cavity combiner has been widely used, the design of the passive combiner circuit is not yet well defined with respect to developing a closed form solution for the impedance presented to each individual IMPATT diode for any order and size combiner. Various techniques such as impedance, S-parameter, and transmission matrix modelling have been used with good results on low order (i.e. $TM_{010}$) combiners employing only a few IMPATT diode circuits. However, for higher-order combiners with a large number of diode circuits, the existing models are not accurate enough and are used only for initial design. The final design is usually derived by empirical adjustment of certain combiner parameters. Another factor affecting optimal $TM_{ono}$ combiner design is achieving maximum combining efficiency which is indirectly related to the combiner impedance response. The specific areas of investigation to be presented include cylindrical resonant cavity combiner theory (Chapter II), cylindrical resonant cavity modelling (Chapter III), and the characterization and test of a $TM_{020}$ test combiner (Chapter IV). The summary and conclusions are subsequently presented in Chapter V.

# CHAPTER II

## CYLINDRICAL RESONANT CAVITY COMBINER THEORY

### General Characteristics

A $TM_{ono}$ combiner as shown in Figure 1 consists of several IMPATT diode circuits located around the periphery of a cylindrical cavity which resonates in a $TM_{ono}$ mode. Resonant cavity combiners may operate as reflection amplifiers, injection-locked oscillators, or free running oscillators depending on circuit design conditions. Operating as an amplifier a circulator must be used with the resonant combiner to isolate input and output. As an amplifier, RF energy is coupled to the cavity $TM_{ono}$ E-field through a probe located at the cavity center and correspondingly to each diode circuit via the cavity H-field which circulates circumferentially within the cavity. The amplified RF waveform is coupled out of the combiner in the reverse order. As an oscillator, the IMPATT diode circuits act as individual sources which are combined and locked in frequency through reactive pulling to the cavity resonant frequency. A $TM_{ono}$ combiner has N+1 resonant frequencies for each mode in which oscillation may occur with only one of these being the desired resonant mode. Thus for proper operation, a cavity with a reasonably high Q must be used to synchronize the diode circuits. An alternative method for obtaining synchronous operation is injection-locking. In injection-locking, frequency synchronization at the cavity frequency is

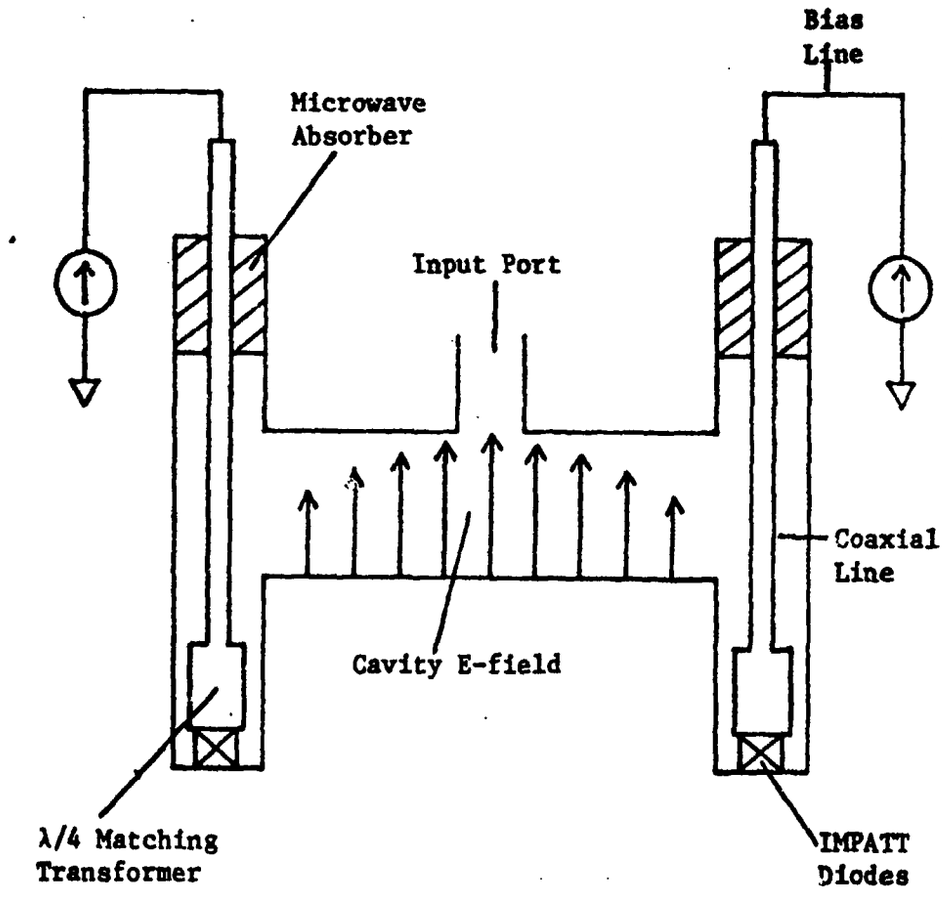


Figure 1. Cross Section of a $TM_{ono}$ Cylindrical Resonant Cavity Combiner

obtained by using a low level RF input to which the diode circuits lock in frequency. Again a circulator must be used to isolate input and output. The cylindrical resonant cavity in all cases performs the functions of distribution or combining of RF power and also operates as a tuned circuit or bandpass filter due to its resonant characteristic.

## The Cylindrical Resonant Cavity

The cylindrical resonant cavity is the basic microwave circuit element of a cylindrical resonant combiner. A cylindrical resonant cavity may be formed by placing metallic ends on a short section of circular waveguide. The solution for the fields existing within a cylindrical resonant cavity can be found in several books [3,8]. The solution proceeds by solving for the cylindrical wave equation with the assumption that there is an initial induced electromagnetic field and that the cavity is a lossless medium containing no charge. The resultant fields that are established are designated as either $TM_{mnq}$ or $TE_{mnq}$ modes where the m, n, and q subscripts refer to the angular, radial, and longitudinal variations within the cavity. In developing the cylindrical resonant combiner, Harp and Stover chose to limit the operation of their combiner to the $TM_{ono}$ mode where n=1,2,... . They did so because the field variations of this set of modes as shown in Figure 2 were correct for coupling to a center probe and to a number of coaxial circuits at the periphery of the cavity. In general, modes with longitudinal variation may be eliminated from consideration by proper choice of cavity length, leaving $TM_{mno}$ and $TE_{mno}$ modes where

m=0,1,2,... and n=1,2,... . Two of the $TM_{mno}$ modes are shown in Figure 3. Note that the E-field maximums of these modes do not occur at the cavity center but the H-field of these modes continues to circulate around the cavity wall. There exist an infinite number of these modes as well and their resonant frequencies are determined from the following equations,

$$f_r(TM_{mno}) = \frac{1}{2\pi\sqrt{\mu\epsilon}} \cdot \frac{\chi_{mn}}{a} \qquad (1)$$

$$f_r(TE_{mno}) = \frac{1}{2\pi\sqrt{\mu\epsilon}} \cdot \frac{\chi'_{mn}}{a} \qquad (2)$$

where a=cavity radius

$\chi_{mn}$=nth zero of the mth order Bessel function $J_m(\chi_{mn})$

$\chi'_{mn}$=nth zero of the mth order Bessel function $J'_m(\chi_{mn})$.

Tables 1 and 2 provide representative values for these zeroes which may be found for example in Tables of Functions by Jahnke and Emde [16]. By comparison of Tables 1 and 2, it may be noted that there are several frequencies where the $TM_{mno}$ and $TE_{mno}$ modes overlap. By selecting m=0 and n=1,2,... various $TM_{ono}$ modes can exist within a cylindrical cavity. Only the $TM_{010}$, $TM_{020}$, and $TM_{040}$ modes have been used in cylindrical cavity combiner designs [4-7] to date. The resonant frequency then for a $TM_{ono}$ mode would be determined from equation (1) by substituting a value for $\chi_{on}$. From equation (1), for a constant resonant frequency, a larger radius cavity and a larger number of diode coaxial circuits may be obtained by using a higher order $TM_{ono}$ mode(i.e. n>1). There are difficulties in doing this, however, because the frequency

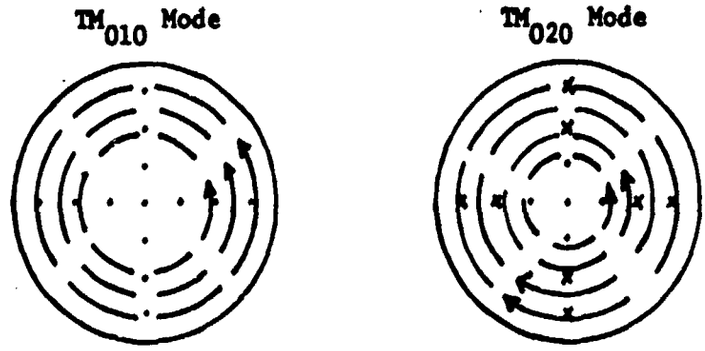


Figure 2. $TM_{ono}$ Mode Field Configurations. E-field . x, H-field +.

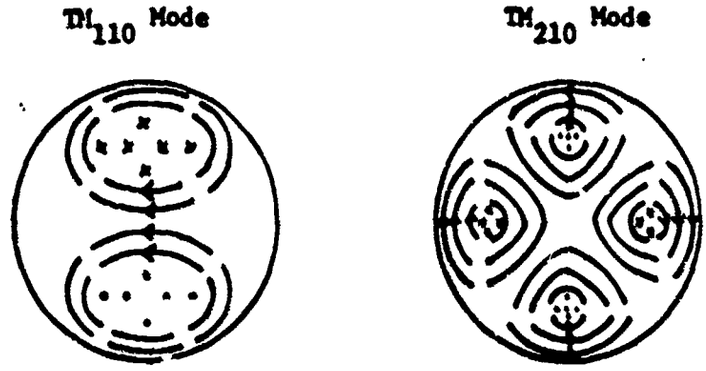


Figure 3. $TM_{mno}$ Mode Field Configurations. E-field . x, H-field +.

TABLE 1. Ordered Zeroes $\chi_{mn}$ of $J_m(\chi_{mn})$

| n \ m | 0 | 1 | 2 | 3 | 4 | 5 |
|---|---|---|---|---|---|---|
| 1 | 2.405 | 3.832 | 5.136 | 6.380 | 7.588 | 8.771 |
| 2 | 5.520 | 7.016 | 8.417 | 9.761 | 11.065 | 12.339 |
| 3 | 8.654 | 10.173 | 11.620 | 13.015 | 14.372 | 15.700 |
| 4 | 11.792 | 13.324 | 14.796 | 16.223 | 17.616 | 18.980 |

TABLE 2. Ordered Zeroes $\chi'_{mn}$ of $J'_m(\chi'_{mn})$

| n \ m | 0 | 1 | 2 | 3 | 4 | 5 |
|---|---|---|---|---|---|---|
| 1 | 3.832 | 1.841 | 3.054 | 4.201 | 5.317 | 6.416 |
| 2 | 7.016 | 5.331 | 6.706 | 8.015 | 9.282 | 10.520 |
| 3 | 10.173 | 8.536 | 9.969 | 11.346 | 12.682 | 13.987 |
| 4 | 13.324 | 11.706 | 13.170 | - | - | - |

separation between adjacent $TM_{mno}$ modes as shown in Figure 4 becomes smaller as n increases. Researchers who have addressed this problem [5,7] have applied mode suppression techniques in their combiner designs. These techniques, although effective in suppressing undesired modes, do increase the loss in a combiner or conversely its combining efficiency. For the $TM_{ono}$ mode, the field variations are presented as

$$E_z = E_o J_o\left(\frac{\chi_{on}}{a} r\right) \tag{3}$$

$$H_\phi = j \frac{E_o}{\eta} J_1\left(\frac{\chi_{on}}{a} r\right) \tag{4}$$

where the time harmonic variation has been suppressed. From close inspection of these two equations, it can be seen that the E-field has only a z-component and varies as a function of r with a maximum intensity at the cavity center. The H-field has only a $\phi$-component and also varies as a function of r with a maximum near the cavity side wall. Because a $TM_{ono}$ mode has no $\phi$ variation, the placement of IMPATT diodes is not critical and the number of diodes which can be used in a cylindrical combiner is limited by factors such as circumferential length and diode package size, power dissipation, and isolation between diode circuits. The $TM_{mno}$ modes have similar variation with respect to radius but also have angular variation as well (see Figure 3). In the design of a cylindrical resonant combiner, it is highly desirable to achieve single mode operation (i.e. a single $TM_{ono}$ mode). IMPATT diodes can resonate at their own avalanche frequencies

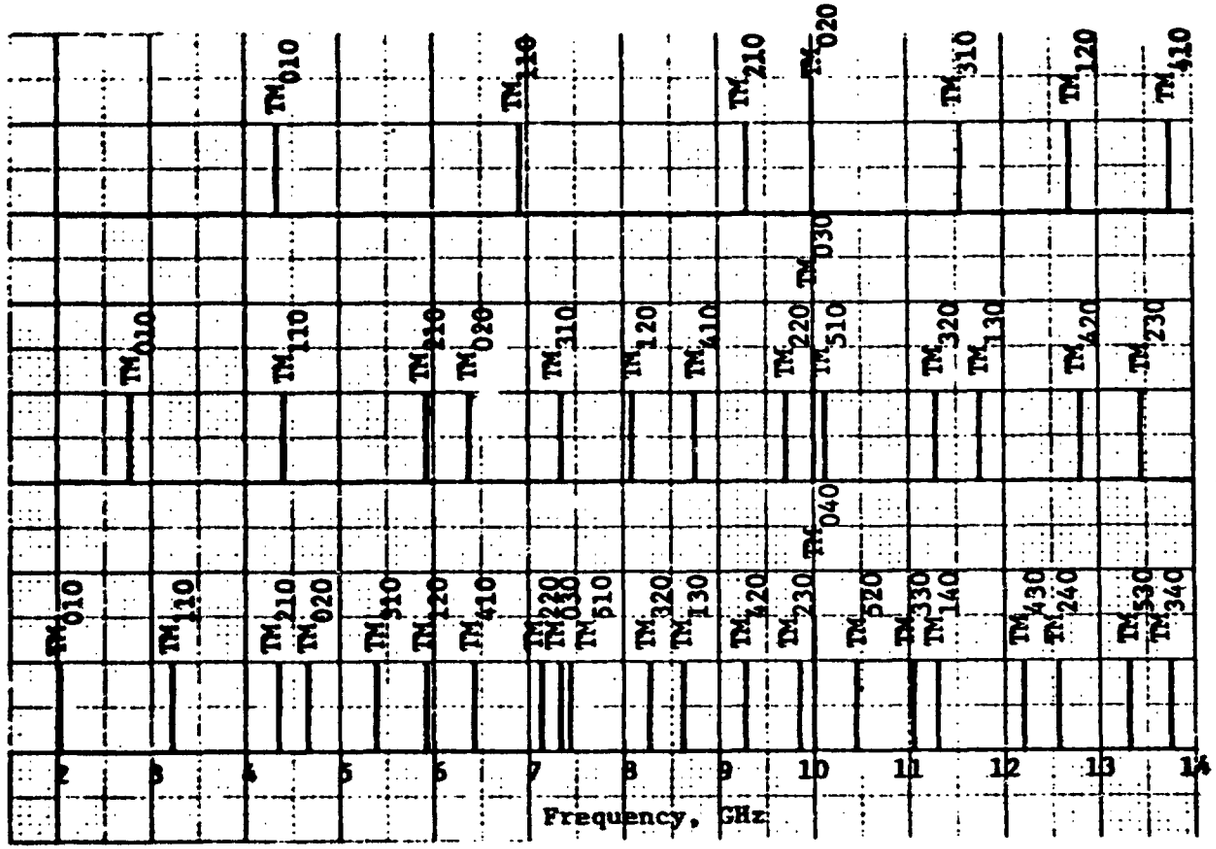


**Figure 4.** Relative Separation Between Various $TM_{mno}$ Modes. The subscript n was increased from 2-4 with each $TM_{ono}$ mode being given a center frequency of 10 GHz.

as a part of the coaxial circuits or they may be synchronized to one of the nonsymmetrical $TM_{mno}$ modes. If an IMPATT diode resonates in one of these modes, not only will RF power generated by that diode not couple to the external circuit but the diode may become unstable in that mode and result in failure. When the IMPATT diodes of a multidiode cavity combiner resonate into their own loads, the output RF spectrum shows distinct resonant lines [6,7] and the output power thus achieved is not useful for amplification or as a source of RF power. Thus to achieve single mode operation, a resonant combiner must employ a high Q cavity which gives this type of combiner a characteristic of being a narrowband amplifier or tunable source. The unloaded Q of a cylindrical resonant cavity may be found by taking the ratio of the energy stored in the cavity to the power dissipated in the cavity walls per cycle times $2\pi$. The unloaded Q for a $TM_{mno}$ or $TM_{ono}$ mode is given by [3,8],

$$Q_u = \frac{\eta \chi_{mn}}{2R_s(1+2/d)} \tag{5}$$

where $\eta$=intrinsic wave impedance= $120\pi$ ohms,

$R_s$=skin resistance, and

d=cavity height.

From inspection of this equation, it can be noted that the unloaded cavity Q of a $TM_{mno}$ or $TM_{ono}$ mode is directly proportional to the order of the mode but inversely proportional to the cavity radius for a given cavity height. The unloaded cavity Q is also inversely proportional to the square root of frequency.

## Coaxial Diode Circuits

The diode circuits in a cylindrical resonant combiner each consist of an IMPATT diode and impedance matching transformer placed at one end of a coaxial transmission line with a bias feed and microwave absorber load placed at the opposite end. The purpose of the impedance matching transformer is to match the impedance of the combiner circuit which includes the cavity and microwave absorber load responses plus the impedance of the other coaxial lines reflected through the cavity to the small impedance of the IMPATT diode. The impedance of a packaged IMPATT diode typically has a negative resistance component on the order of -1 ohms and a inductive reactance component of approximately 6-8 ohms. The microwave absorber functions as a stabilizing load for the IMPATT diode at frequencies away for the desired $TM_{ono}$ mode. In other words to eliminate runaway oscillations, the positive circuit resistance must be greater than or equal to the magnitude of the negative IMPATT resistance. In operation, standing voltage and current waves exist on the coaxial lines and if the microwave absorber load position is adjusted so that a current maximum is located at the cavity midplane, then maximum power transfer from the coaxial lines to the cavity or vice versa occurs. This maximum power transfer occurs because the standing current wave easily couples to the H-field of the cavity. The magnitude of the standing waves and hence the fraction of power transferred to the cavity can be controlled by the shape of the microwave absorber. Various geometries of the microwave absorber such as flat, partial taper, and full taper as shown in Figure 5 have been investigated [4-7]. The flat termination

has been found to provide the best power transfer or combining efficiency but is narrowband while the fully tapered termination results in a poor combining efficiency and has the broadest bandwidth. Microwave designers have implemented partially tapered terminations to achieve moderate bandwidths while maintaining acceptable efficiency. The equations describing the impedance presented to an IMPATT are shown later in Chapter III.

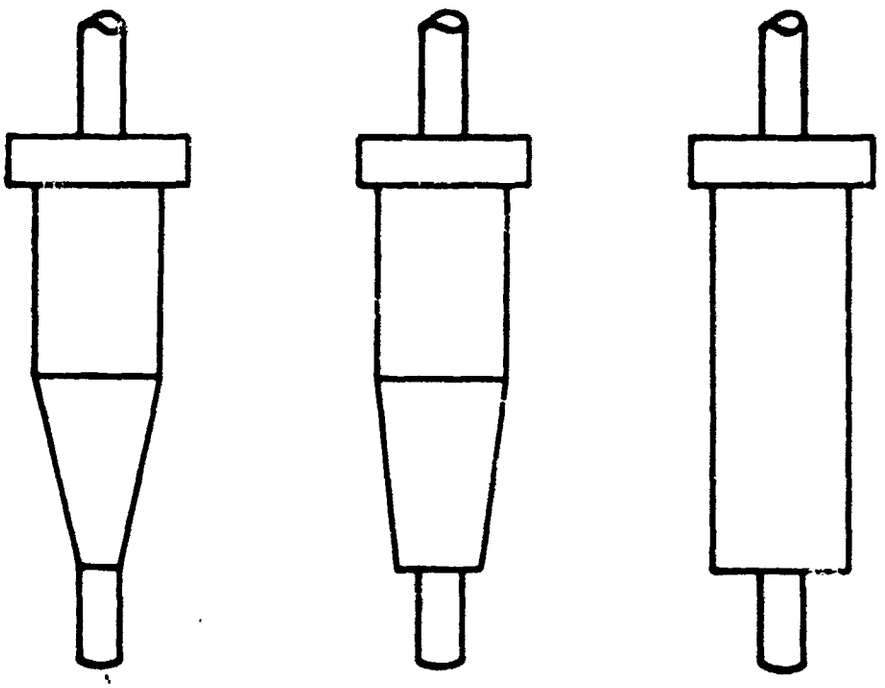

FULL TAPER PARTIAL TAPER FLAT

Figure 5. Various Microwave Absorber Load Geometries

## CHAPTER III

## CYLINDRICAL RESONANT CAVITY COMBINER MODELLING

There are several approaches (e.g. empirical [5], impedance [2,6], S-parameter [7], and transmission matrix modelling schemes) including combinations of these which have been applied to modelling an N-diode $TM_{onO}$ cylindrical resonant cavity combiner to date. The most widely used model is the Kurokawa combiner model [2] which is based upon determining the impedance(admittance) presented to an IMPATT diode by an N+1 port network with the circuit operating as a free running oscillator. However, the full potential of cylindrical resonant combiners employing IMPATT diodes has not been realized with the existing combiner models. This occurs for several reasons. First, the $TM_{ono}$ combiners have primarily been designed to operate as free running or injection-locked oscillators due to the Kurokawa model. In general though, the circuit conditions for optimal performance of a combiner as an oscillator differ from those for amplifier operation. As an oscillator, condiderations such as frequency stability, oscillator FM noise, and tunability are important while gain and bandwidth are predominant in amplifier operation. In both cases, circuit efficiency is of importance. The circuit requirements for an oscillator are such that when the frequency is varied, the power output should remain constant. However for an amplifier, as the input frequency varies

at a given power level, the gain should remain constant over the bandwidth of the amplifier. From the circuit viewpoint, this requires the device impedance line and the circuit impedance line to track one another. Thus, a more accurate $TM_{ono}$ combiner model should be able to include amplifier operation as well. This investigation has not emphasized developing a new combiner model but rather the study and characterization of $TM_{ono}$ combiners to improve the existing Kurokawa model. Secondly, the equivalent circuit components of the Kurokawa model(e.g. the coupling coefficients) are not accessible to direct external measurement and usually must be calculated or approximated. Lastly, the Kurokawa combiner model considers the combiner to be a symmetric N+1 port network with no coupling interaction between pairs of diode circuits. It has been found [7] that when the number of diode circuits increases beyond approximately 4-8, that mutual coupling effects begin to occur. The modelling of mutual coupling effects, however, is presently too complex and is not included in this investigation. This chapter is generally concerned with examining the Kurokawa combiner model which has been applied frequently to $TM_{ono}$ combiners and determining relations for some of its components. In particular the topics to be discussed are general modelling of two-port resonant cavities, the Kurokawa combiner model, and equivalent circuit impedance relations for a $TM_{ono}$ combiner.

## General Modelling of Two-Port Resonant Cavities

Microwave cavities are inherently very complex networks with an infinite number of natural resonant frequencies and may be modelled

with either lumped equivalent circuits or as distributed transmission lines bounded by known discontinuities [10]. In this section a very general lumped element representation will first be presented and will be followed by a single mode lumped element network model.

General Representation of Lossless Two-Port Resonant Networks

In its most general form a two-port lossless microwave cavity may be represented by the network shown in Figure 6. This circuit, as shown by Ragan [11] and Beringer [12], is derived by extending Foster's Reactance Theorem to a lossless two-port network and leads to the following open circuit reactances.

$$X_{11}(\omega) = \omega L_{10} - \frac{1}{\omega C_{10}} + \sum_{k=1}^{\infty} \frac{\omega^3 M_{1k}^2}{L_k(\omega_k^2 - \omega^2)} \tag{6}$$

$$X_{22}(\omega) = \omega L_{20} - \frac{1}{\omega C_{20}} + \sum_{k=1}^{\infty} \frac{\omega^3 M_{2k}^2}{L_k(\omega_k^2 - \omega^2)} \tag{7}$$

$$X_{12}(\omega) = \omega M_0 - \frac{1}{\omega C_{m0}} + \sum_{k=1}^{\infty} \frac{\omega^3 M_{1k} M_{2k}}{L_k(\omega_k^2 - \omega^2)} \tag{8}$$

Each resonant loop in this network represents one of the natural resonant modes of the cavity and the capacitors and the ideal transformer together represent direct capacitive coupling between the input and output terminals. Practical microwave cavities are not lossless and the dissipation in the cavity may be accounted for by including a series resistor in each resonant loop in the equivalent circuit of Figure 6. To account for this series resistance in equations (6-8), an additional

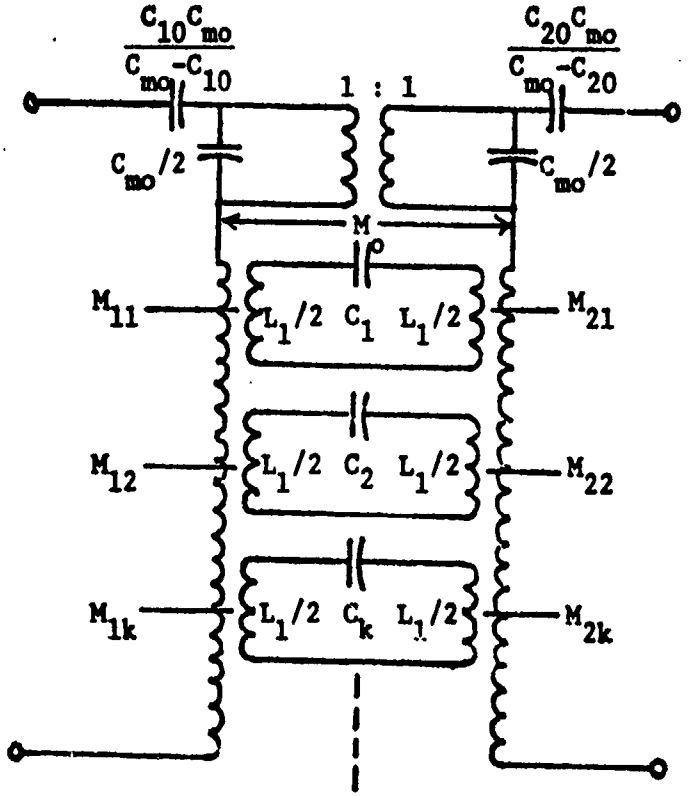


Figure 6. Equivalent Circuit of a General Lossless Two-Port Resonant Cavity

term should be included in the denominator of the summations. As can be noted, the equivalent circuit of the cavity modes is described by series RLC circuits. Likewise, the cavity modes may be represented by shunt RLC circuits. The choice of which equivalent circuit to use is determined by the reference plane of measuremnet [9]. There are two terms (i.e. either the detuned short-circuit position or the detuned open-circuit position) which are used in the description of the reference plane position. The detuned short- or open-circuit impedances are defined as the impedance of the network when excited at a frequency far removed from the resonant frequency of the network. If the detuned short circuit position were used, the shunt RLC circuit would be appropriate while the series RLC would be correct when the detuned open-circuit position was used. With respect to the cylindrical resonant cavity combiner, the equivalent circuit of Figure 6 represents all of the $TM_{mno}$ modes possible. However, the two-port configuration is not representative of an N+1 port combiner except when the combiner is considered to be symmetrical.

Single-Mode Lumped Element Two-Port Resonant Network Model

As stated earlier, $TM_{ono}$ combiners employ relatively high Q cylindrical resonant cavities which are designed to operate in a single $TM_{ono}$ mode. Each of the infinite resonant modes of the cavity still exist if stimulated but are assumed to be sufficiently removed from the desired mode so that their equivalent resonant circuits may be removed from consideration. Also, the direct coupling elements may be removed if found to be small enough. In a $TM_{o,o}$ combiner, the direct coupling is assumed to be small because the center probe and coaxial lines are

not in close proximity. The result is an equivalent circuit which is composed of a single series RLC or shunt RLC circuit representing a particualr $TM_{ono}$ mode with ideal transformers representing the coupling of the input and output circuits as shown in Figure 7. The shunt RLC resonant circuit and ideal transformers are used in a classic paper by Kurokawa to model a resonant waveguide combiner which is discussed later. Before describing the Kurokawa model, the Q factors (i.e. the loaded, external, and unloaded Q's) of a two-port lumped element resonant network are given.

Q Factors of a Lossless Two-Port Resonant Network

Consider a single-mode lumped element resonant network as shown in Figure 7 below which represents a cavity coupling system with matched input and output impedances $Z_o$ and $Z_L$. For a $TM_{ono}$ combiner, $Z_o$ would be the external impedance presented to the combiner and $Z_L$ would represent the IMPATT diode circuit impedances in parallel for a symmetric combiner.

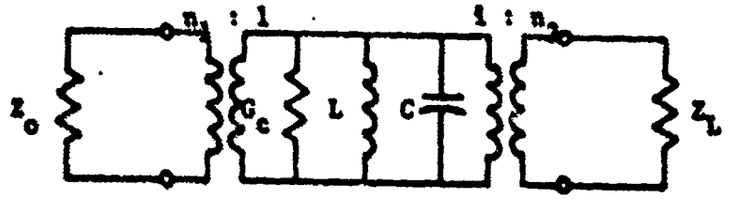


Figure 7. Single-Mode Resonant Cavity Equivalent Circuit

The coupling elements are assumed to be lossless (i.e. because any loss may be cancelled by suitable choice of reference planes) and no interaction between them is assumed to occur. Transforming the generator and load circuits to the resonant circuit, the loaded Q of the network is easily determined as,

$$Q_L = \frac{Q_0}{1 + \frac{n_1^2}{Z_0 G_c} + \frac{n_2^2}{Z_L G_c}} = \frac{Q_e}{1 + \beta_1 + \beta_2} \qquad (9)$$

where $Q_e = \omega_0 C / G_c$

The external Q, $Q_{ex}$, is the Q of the external network only and for the circuit of Figure 7, it is defined as,

$$Q_{ex} = \frac{\omega_0 C / G_c}{\frac{n_1^2}{Z_0 G_c} + \frac{n_2^2}{Z_L G_c}} = \frac{Q_e}{\beta_1 + \beta_2} \qquad (10)$$

## The Kurokawa Combiner Model

Kurokawa in 1971 presented a paper on "The Single-Cavity Multiple-Device Oscillator" [2] which has been referenced and used by many researchers in the combiner area to model $TM_{ono}$ cylindrical resonant cavity combiners. His model is derived from the theory already presented in this chapter except that the circuit he uses (i.e. an N+1 port) is much more complex. He uses a single shunt RLC circuit to represent the resonant cavity (i.e. a waveguide cavity) and lossless ideal transformers to represent coupling to the cavity. The diode circuits he uses are identical to those used in a $TM_{ono}$ combiner. Kurokawa takes the approach of solving for the eigenvalue equations for the network admittance facing each IMPATT diode when the combiner

is operated as a free running oscillator. Namely when,

$$Y_N = NY_D \tag{11}$$

where $Y_N$ represents the admittance of the N-port network and $Y_D$ represents the admittance of a single IMPATT diode. Kurokawa assumes equal coupling to all the diode circuits and neglects any coupling between pairs of diode circuits through the resonant cavity. In Kurokawa's circuit(i.e. a rectangular waveguide combiner), this assumption is correct because each diode circuit must be spaced by half wavelengths for maximum coupling to the waveguide H-field. However, the same is not true in a $TM_{ono}$ combiner where the spacing is not wavelength dependent and isolation between each diode circuit decreases significantly with an increasing number of diode circuits. When the isolation between diode circuits in a $TM_{ono}$ combiner becomes too small, the RF voltage amplitudes of each diode circuit, which are not necessarily in phase, will cause single or pairs of diodes to resonate at frequencies independent of the cavity resonant frequency. As stated earlier, these mutual coupling effects will not be treated here. Kurokawa also discusses the circuit conditions for suppressing undesired modes, stable operation, and injection-locking and presents equations on circuit efficiency and noise performance. In the section on suppressing undesired modes, Kurokawa stated that the coupling coefficient for other modes will be considerably smaller than for the desired mode, thus, eliminating any moding problems. However, it has been noted by Mastroianni [6] and in this investigation that matched coupling can occur simultaneously to more than one mode for certain circuit conditions. Thus, IMPATT diode operation in an undesired $TM_{mno}$ mode is

certainly possible. Kurokawa, in his model, uses a tapered microwave absorber load which gave his design excellent stability (i.e. a tapered load causes matched coupling of all modes) in a single mode. The tapered load, however, resulted in poor combining efficiency. Because Kurokawa uses a tapered load, he describes the load as a constant equal to the characteristic impedance of a 50 ohm coaxial air line which in the general case it is not. Impedance relations were developed for a flat microwave absorber load and are presented later in Chapter III. The measured versus calculated impedance of a microwave absorber load is presented in Chapter IV.

## $TM_{ono}$ Combiner Equivalent Circuit Impedance Relations

In this section, the equivalent circuit relations for a $TM_{ono}$ combiner which is based upon the Kurokawa model are presented. The impedance presented to an IMPATT diode will later be computed using this model and then compared to the measured results in Chapter IV to test the applicability of the Kurokawa model. Other approaches to modelling a $TM_{ono}$ combiner (i.e. using S-parameters) were considered but S-parameter modelling, in general, does not provide the microwave designer with the information necessary to predict combiner performance as a function of circuit parameters. The $TM_{020}$ mode was selected in this investigation so that circuit interaction with modes other than the desired mode could be characterized. The $TM_{020}$ combiner equivalent circuit is presented in Figure 8. The circuit is a single-mode N+1 port resonant network.

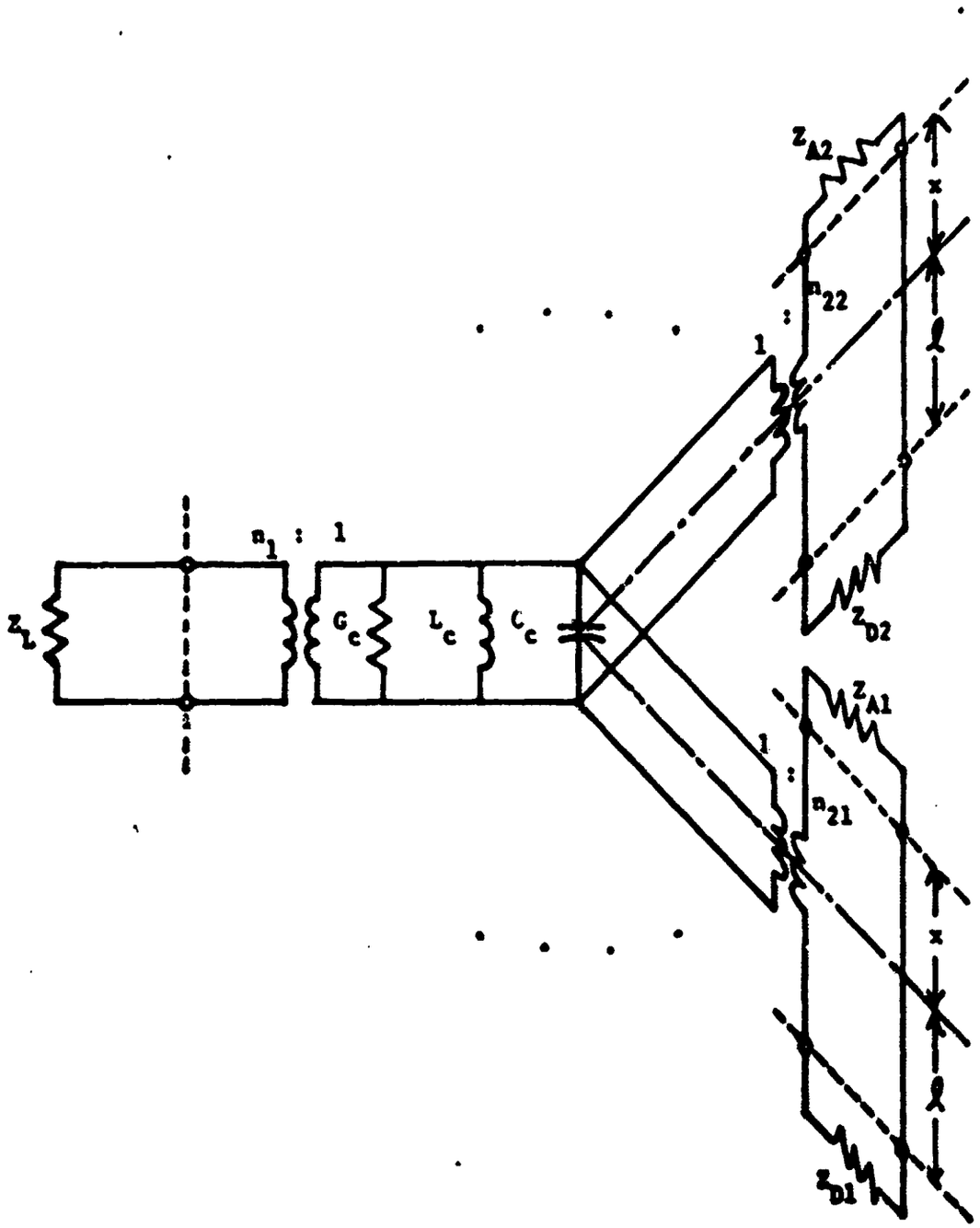


Figure 8. Equivalent Circuit of a $TN_{ONO}$ Combiner with N Coaxial Lines

## Impedance Presented to an IMPATT Diode

For the symmetric single-mode $TM_{ono}$ combiner equivalent circuit shown in Figure 8, the impedance presented to an IMPATT diode by the network is described. As stated before, the impedance presented to the diode is based on the oscillator condition. The impedance presented to an IMPATT diode can be determined at the diode plane or at the cavity midplane. If the network impedance is determined at the cavity midplane, it is equated to a transformed diode impedance (i.e. the impedance of the diode transformed through the matching transformer and a section of coaxial line). The impedance of the combiner network at the cavity midplane can be shown to be,

$$Z_N = Z_A + \frac{Nn_2^2}{\sqrt{\frac{C_c}{L_c}}\left[\frac{1}{Q_c} + \frac{1}{Q_E} + j\left(\frac{f}{f_c} - \frac{f_c}{f}\right)\right]} \tag{12}$$

where $Z_A$=microwave absorber impedance

N=number of diode circuits

$Q_c$=unloaded cavity Q

$Q_E$=external Q

Next, the impedance presented to an IMPATT diode is determined by transforming $Z_N$ through a short 50 ohm section of line and a $\lambda/4$ transformer. The impedance presented to the $\lambda/4$ transformer is determined from

$$Z_N' = Z_o \frac{Z_N + jZ_o \tan\beta l}{Z_o + jZ_N \tan\beta l} \tag{13}$$

where $\ell$ is the length of line between the cavity midplane and the $\lambda/4$ transformer. A calculator program to generate this impedance was developed and is provided in Appendix B. The network impedance which is equated to the diode impedance is subsequently determined using,

$$Z_D = Z_T^2 / Z_N' \tag{14}$$

where $Z_T$= $\lambda/4$ transformer impedance.

The matching transformer impedance, $Z_T$, is calculated using,

$$Z_T = \frac{60}{\sqrt{\epsilon_r}} \ln \frac{b}{a} \tag{15}$$

where b= radius of the coaxial line outer conductor,

a= radius of the coaxial line center conductor, and

$\epsilon_r$= dielectric permittivity constant.

A program callen ZCOMB, provided in Appendix A, was written to calculate representative values of $Z_N'$ as a function of frequency for later comparison to the measured data.

### Resonant Circuit Element Relations

Before the impedance presented to the IMPATT diode can be calculated, the relations for the resonant circuit elements must be known. The conductance of the resonant cavity may be shown to be [8],

$$G_c = \frac{2\pi a/d(1+a/d)R_s J_1^2(\chi_{mn})}{\eta^2}, \tag{16}$$

which is determined from consideration of the dissipated power in the cavity. Using the equation for unloaded cavity Q (i.e. $Q=\omega_o C_c/G_c$), the resonant cavity capacitance can be described as,

$$C_c = \frac{\pi a/d\, \chi_{mn} J_1^2(\chi_{mn})}{\eta} \quad . \tag{17}$$

Following this, the equation for the resonant cavity inductance is found from $\omega_o^2 = 1/LC$. The inductance is,

$$L_c = \frac{1}{\omega^2} \cdot \frac{\eta}{\pi a/d\, \chi_{mn} J_1^2(\chi_{mn})} \quad . \tag{18}$$

Lastly for use in equation (12), the equation for $\sqrt{C_c/L_c}$ is,

$$\sqrt{\frac{C_c}{L_c}} = \omega_c C_c = \frac{\pi \omega a/d\, \chi_{mn} J_1^2(\chi_{mn})}{\eta} \quad . \tag{19}$$

Microwave Absorber Impedance Relations

The microwave absorber or stabilization load which terminates the diode line can be viewed as an infinite coaxial transmission line (i.e. due to the significant attenuation characteristic of the absorber) with complex values of permittivity and permeability. The microwave absorber is a composition of iron and expoxy called ECCOSORB MF 116 [17]. The complex values of permittivity and permeability are needed because of the electric and magnetic properties of the ECCOSORB material. The general relation for the characteristic impedance of a distributed transmission line can be used to describe this impedance and is given as,

$$Z_A = \sqrt{\frac{R + j\omega L}{G + j\omega C}} \tag{20}$$

The individual components of equation (20) can be determined from static fields and are defined as,

$$R = \frac{R_s}{2\pi}\cdot\left(\frac{1}{b}+\frac{1}{a}\right) \quad \text{ohms/meter} \tag{21}$$

$$L = \frac{\hat{\mu}}{2\pi}\ln\frac{b}{a} \quad \text{henrys/meter} \tag{22}$$

$$C = \frac{2\pi\hat{\epsilon}}{\ln\frac{b}{a}} \quad \text{farads/meter} \tag{23}$$

$$G = \frac{2\pi\omega\epsilon_o\epsilon_r''}{\ln\frac{b}{a}} \quad \text{siemens/meter} \tag{24}$$

where $R_s = \sqrt{\pi f \mu/\sigma}$

$\mu = \mu_o(\mu_r' - j\mu_r'')$

$\epsilon = \epsilon_o(\epsilon_r' - j\epsilon_r'')$.

It is also useful to compute the attenuation constant, $\alpha$, for this material which may be computed from,

$$\alpha = Re(\gamma) = Re\left[\sqrt{(R+j\omega L)(G+j\omega C)}\right] \tag{25}$$

with the substitution of equations (21-24). In terms of dB/cm, $\alpha$ is given as,

$$\alpha(dB/cm) = 8.686 \times 10^{-2}\ \alpha(nepers/meter). \tag{26}$$

In the section on measurements, it will be shown that the defining equations for the microwave absorber load are comparatively accurate.

# CHAPTER IV

## $TM_{020}$ TEST COMBINER CHARACTERIZATION

The objective of this chapter is to characterize a $TM_{020}$ test combiner in order to test the applicability of using the Kurokawa modal as proposed by various researchers for modelling higher- order mode multiple diode $TM_{ono}$ combiners. The characterization consists of presenting test data on single- and two-port microwave measurements on a cylindrical resonant cavity test combiner and then correlating the measured impedances of the combiner with calculated impedances.

### $TM_{020}$ Test Combiner Description

By using equation (1), a $TM_{020}$ test combiner was designed with a resonant frequency of 10 GHz. The $TM_{020}$ mode was selected for the design so that the relative interference from other modes (e.g. the $TM_{210}$ mode) could be studied. A cross section of the test combiner is shown in Figure 9. This test combiner has been designed with features that are not included in a typical combiner design. The test combiner has four coaxial lines in which the impedance matching transformers and IMPATT diodes have been replaced with .250" semi-rigid coax and type N coaxial connectors. The length of the coaxial lines was chosen so that later use of IMPATT diodes in the combiner would be possible. With this modification, the impedance presented to an IMPATT diode can be measured. The test combiner also employs moveable flat profile micro-

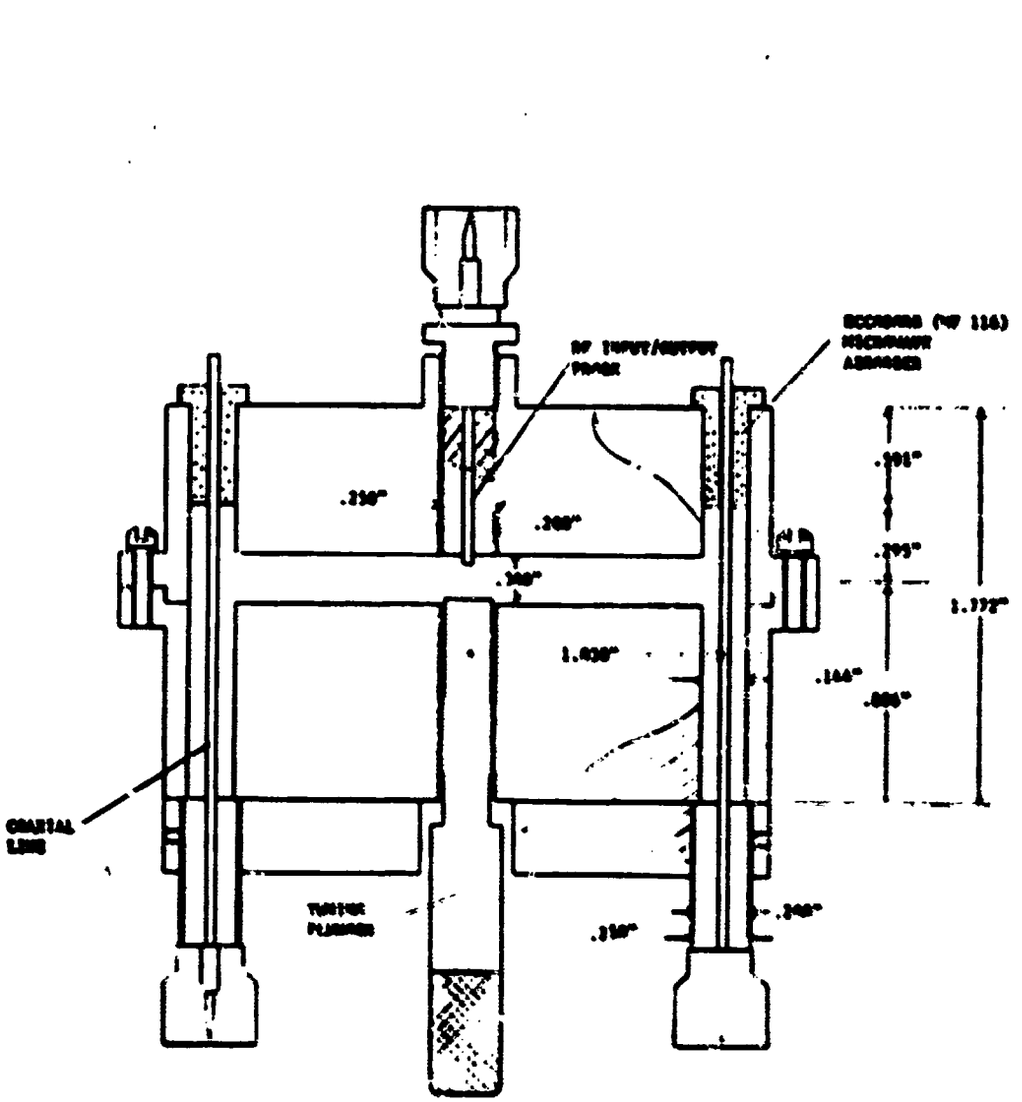


Figure 9. $TM_{020}$ Test Combiner Cross Section

wave absorber terminations and provision is made for adjusting the cavity height to change the Q of the resonant cavity (i.e. with inserts). The microwave absorbers were made from the ECCOSORB MF 116 material described earlier and were designed to be positioned $\lambda/4$ wavelengths from the cavity midplane when fully inserted. The input to the test combiner is also a .250" coaxial line and coupling to the cavity is accomplished via a .025" extension of the center conductor. One additional feature the test combiner has is a .250" frequency tuning plunger which is located opposite to the coaxial input line along the cylindrical cavity axis. Modifications to the existing test combiner for use with IMPATT diodes include replacing the coaxial output lines with diodes mounted on a water cooled copper heatsink and redesigned coaxial center conductors having $\lambda/4$ matching transformers.

## $TM_{020}$ Test Combiner Measurements

The characterization of the test combiner was primarily accomplished using an HP 8545A Automatic Network Analyzer (ANA). A block diagram of the ANA measurement system is shown in Figure 10. Both manual and automatic measurements can be made using the ANA; however, only manual measurements were performed in this investigation due to the requirement for making broadband measurements to observe the test combiner response in several resonant modes. The manual measurements were made by taking outputs from the ANA and recording transmission coefficient and impedance data using an HP 7046A X-Y recorder. These measurements as described in the following paragraphs consist of measuring the test combiner $\eta$, combiner input impedance, combiner

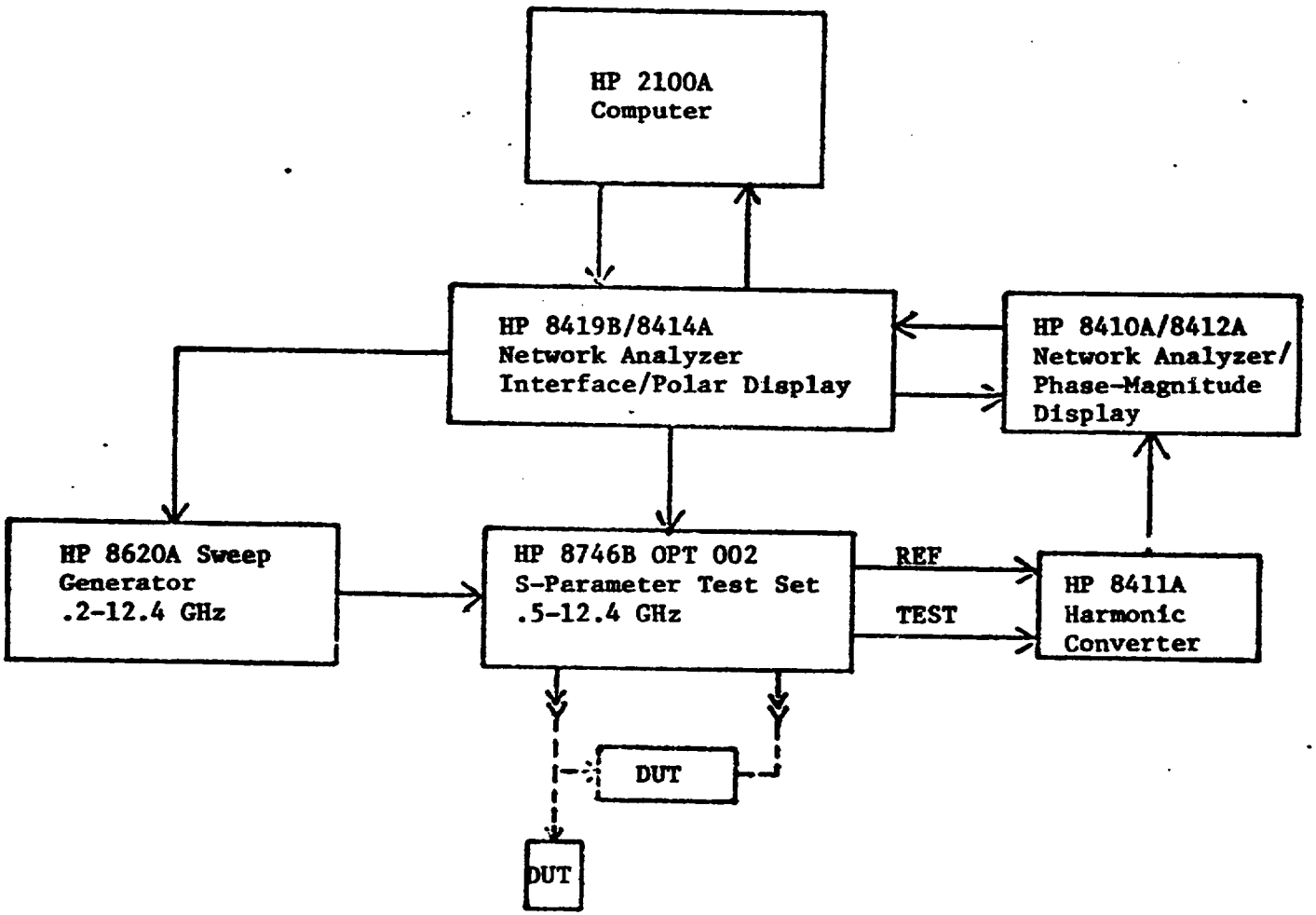


**Figure 10. HP 8545A Automatic Network Analyzer System**

coaxial line impedance, and combiner transmission coefficient.

### Combiner Q Measurements

There are several techniques to measure the Q of a resonant circuit. These techniques can be grouped into transmission methods, impedance measurement methods, transient decay methods, and dynamic methods. Ginzton [9], in his textbook, shows a fairly accurate graphical method of determining the unloaded Q, the external Q, and the loaded Q of a resonant cavity using the Smith chart. His graphical method assumes no coupling loss. The transmission method is the simplest to measure but only the loaded Q of a resonant network may be determined directly. The transient methods, which consist of measuring the decay time of an RF pulse, are also accurate but only when the cavity Q exceeds ∿10,000. Ginzton's graphical method of measuring the $TM_{020}$ test cavity combiner circuit Q's has been used and these values for different cavity heights are shown in Table 3 below.

Table 3. $TM_{020}$ Cavity Test Combiner Measured versus Calculated Q's

| Cavity height, d(in.) | $TM_{020}$ Center frequency (GHz) | $Q_o$ | $Q_E$ | $Q_L$ | $Q_o$(calc.) |
|---|---|---|---|---|---|
| .150 | 9.96 | 800 | 800 | 398 | 3861 |
| .200 | 9.97 | 1108 | 1108 | 498 | 4949 |
| .300 | 9.98 | 2494 | 2494 | 1247 | 6895 |

Note: An effective radius of 1.11 in. was used in calculating $Q_o$.

For the measurements, critical coupling to the cavity was accomplished by adjusting the input probe. Thus, the coupling coefficient $\beta=1$,

$Q_E = Q_o$, and $Q_L = Q_o/2$. The measured Q's as can be noted are much lower than the calculated values. The primary reason for this discrepancy is that additional loss exists at the apertures for the coaxial lines. The coaxial line center conductors were removed to achieve minimum coupling to the lines during the Q measurements. However, the scalloped contour at the cavity/coaxial line interface does increase the losses of the cavity. The graphical method of measuring circuit Q's is shown by the example in Figure 11.

Combiner Input Circuit Measurements

These measurements consist of characterizing the input impedance response of the $TM_{020}$ test combiner under two conditions. The first condition is where all the coaxial line center conductors at the periphery of the cavity are removed. The equivalent circuit of the test combiner then reduces to a single-port shunt resonant network with a single ideal transformer representing the coupling to the cavity (Figure 12). With this modification, the cavity has no additional loading from the coaxial lines and the response of the shunt resonant network shown can be observed. Also, the unloaded and loaded values of circuit Q were obtained this way. The second condition is where all the coaxial lines are present and are terminated in 50 ohm loads in order to duplicate the circuit conditions of an ideal combiner (i.e. one in which there are no mismatch losses). The input impedance for both conditions have been measured with two different cavity heights as shown in Figures 13 and 14. The purpose of varying the cavity height is to affect a change in the unloaded cavity Q. For these measurements, the input probe depth has been adjusted to achieve

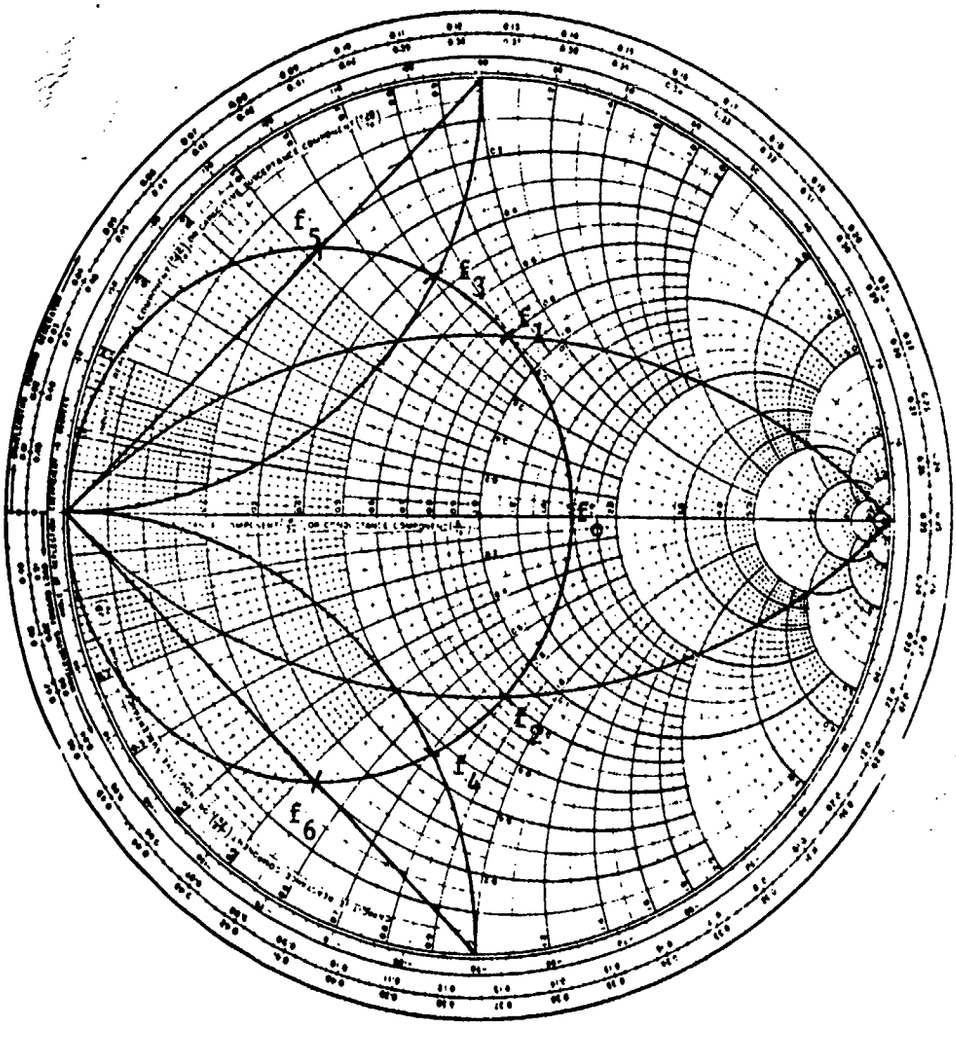


$$Q_o = \frac{f_o}{f_2 - f_1} \qquad Q_E = \frac{f_o}{f_4 - f_3} \qquad Q_L = \frac{f_o}{f_6 - f_5}$$

**Figure 11. Graphical Method for Measuring Q**

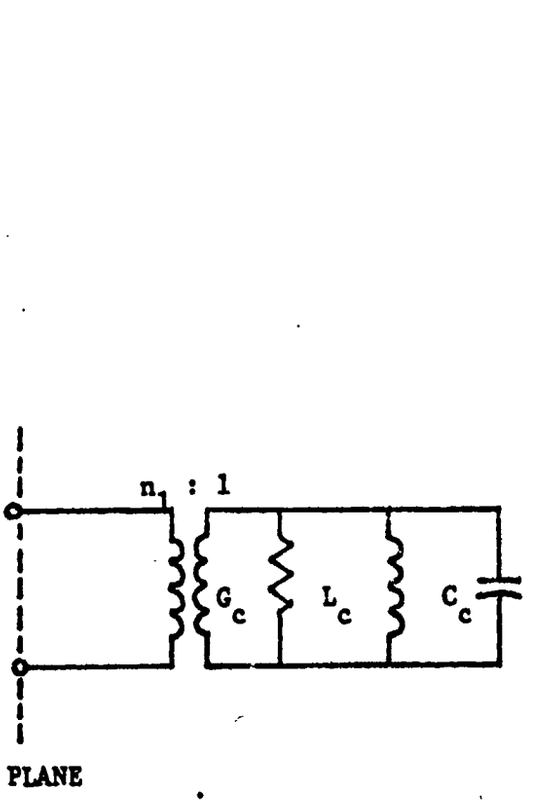


Figure 12. $TM_{ono}$ Combiner Equivalent Circuit with Coaxial Lines Removed

critical coupling at the center frequency of the $TM_{020}$ mode. Also, a reference plane extension on the network analyzer is adjusted so that the input phase to the combiner is correct. When the coaxial lines were in place, the microwave absorber loads were positioned so the standing current wave on each coaxial line would coincide with the cavity/coaxial line aperture for maximum power transfer to the loads in the coaxial lines. The equivalent circuit with coaxial lines is that of Figure 8 and it is expected that the coaxial lines will load down the response of the cavity which it does by looking at Figure 13 or 14. This is because the loaded Q, which is governed by equation (9) where $\beta_2$ represents the coaxial line coupling coefficient, decreases. For the .150" high cavity, the center frequency of the $TM_{020}$ mode was 9.96 GHz with no coaxial lines present and decreased to 9.82 GHz when the coaxial lines were included. The center frequency decreased because the center probe had to be inserted further to achieve critical coupling. The resonant frequency of a cylindrical cavity will decrease with any perturbation according to the relation [8],

$$\Delta\omega = -1/2 \frac{\Delta V}{V} \tag{27}$$

where V is the volume of the cavity and $\Delta V$ is the volume of the perturbation. With no coaxial lines the unloaded and loaded cavity Q values were 664 and 332, respectively, and decreased to 240 and 120 with the addition of the coaxial lines which is approximately a 2/3 reduction in Q. With the coaxial lines in place, the microwave absorber loads were positioned 1.385 cm ($\sim\lambda/2$) from the midplane of the cavity. There exists an open circuit at the microwave absorber load,

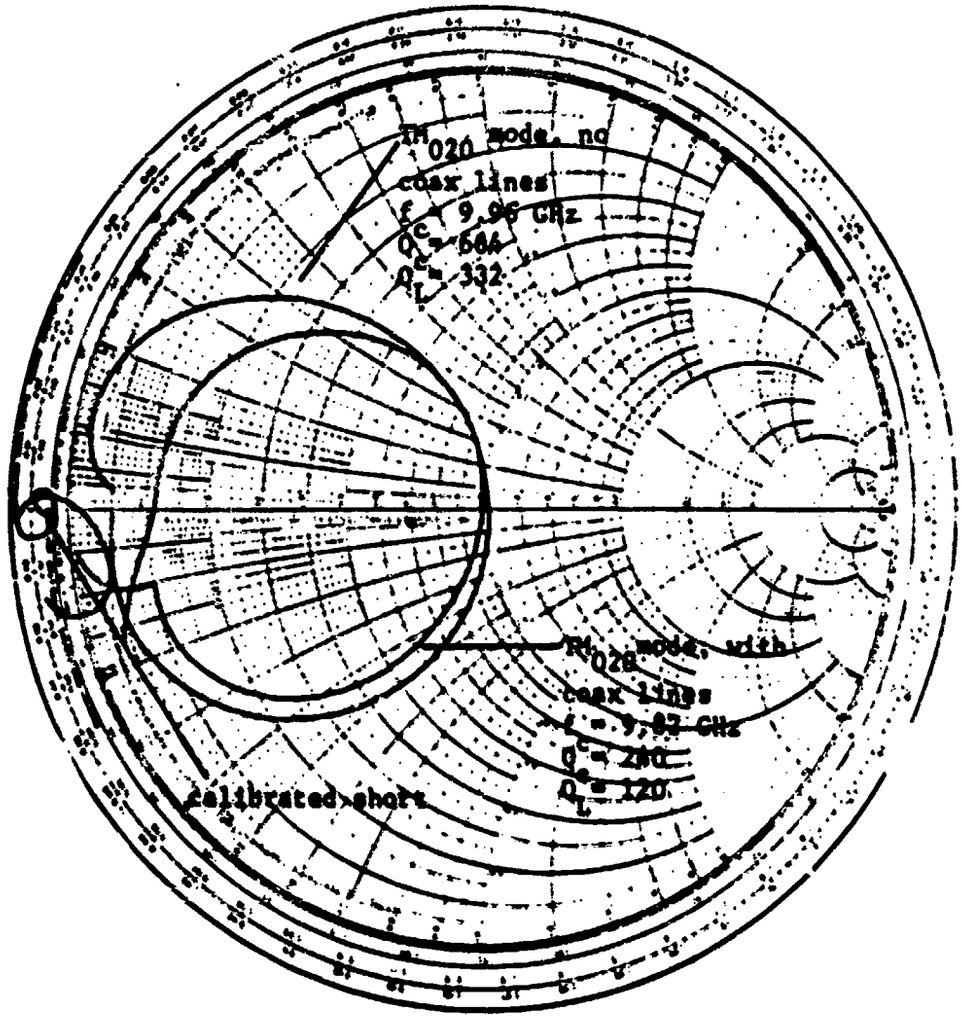


Figure 13. $TM_{020}$ Test Combiner Input Impedance, d=.150"

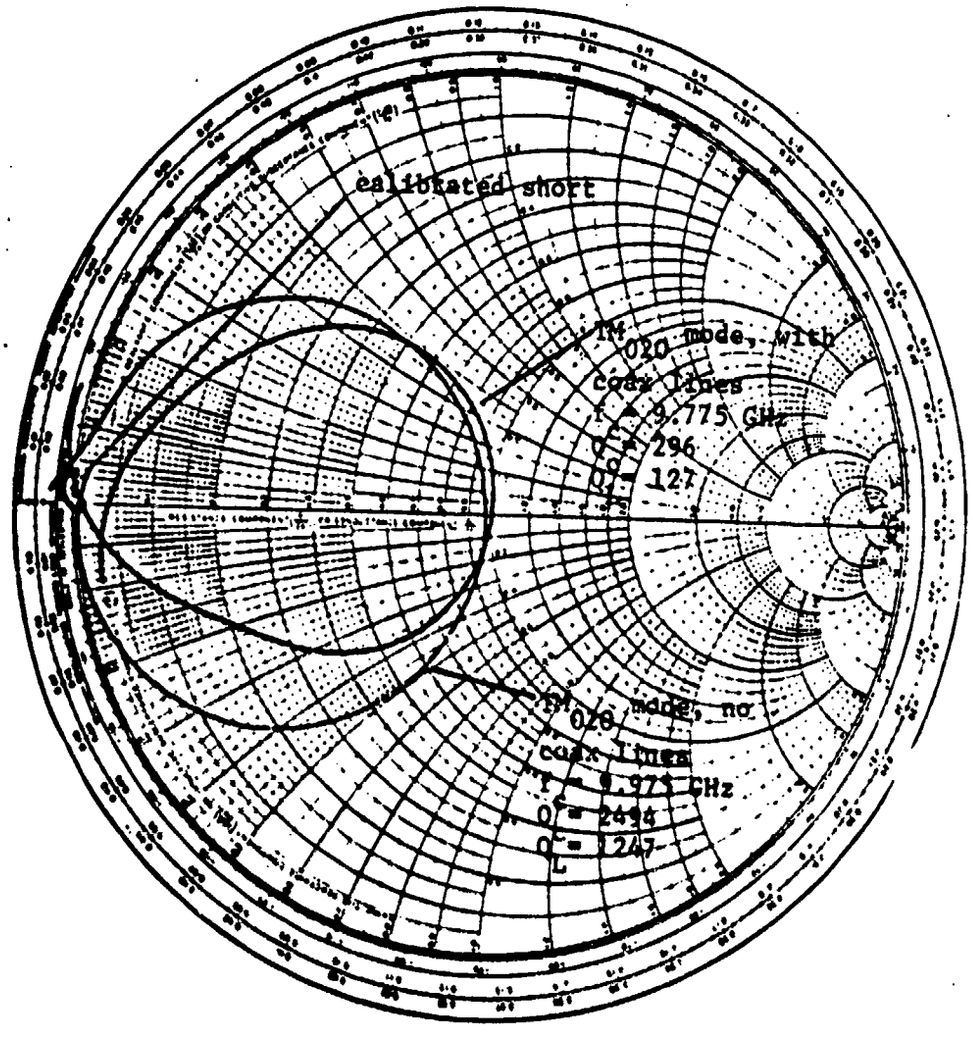


Figure 14. $TM_{020}$ Test Combiner Input Impedance, d=.300"

and thus, a current maximum occurs at $\lambda/2$ wavelengths toward the cavity or at the cavity midplane. Using a .300" high cavity, the center frequency of the $TM_{020}$ mode was 9.975 GHz with no coaxial lines present and decreased to 9.775 GHz with the coaxial lines. The .300" high cavity suffered the greatest change in resonant Q when the coaxial lines were used. The unloaded and loaded Q values were 2494 and 1247, respectively, with no coaxial lines and decreased to approximately 1/10 these values, namely, 296 and 127, when loaded by the coaxial lines. The microwave absorber loads were positoned at 1.623 cm ($\sim\lambda/2$) for the .300" high cavity. For both the .150" and .300" high cavities, the test combiner exhibited significant loading with the addition of the coaxial lines. It is seen in these figures that near the resonant frequency, the impedance response of the cavity circuit elements predominate while away from resonance the impedance does not approach zero but some small value.

## Combiner Coaxial Line Impedance

The test combiner coaxial line measurements consisted of characterizing the impedance response at one of the coaxial lines under several variations. The impedance observed here is the impedance of the combiner network before it is transformed through a 50 ohm section of line and a $\lambda/4$ transformer to the diode plane. Variations in the test combiner circuit such as shorting or matching the cavity center probe, leaving or removing all other coaxial lines, and changing the cavity height were involved in these measurements. The purpose of varying these parameters was to observe the changes in the cavity-to-coaxial line coupling of the $TM_{020}$ and $TM_{210}$ modes. All

the coaxial line measurements were made over approximately the 9.1 to 10.5 GHz frequency range which includes both modes. In the measurements with the center probe present, the probe impedance was critically coupled to the cavity impedance as shown in Figures 13 and 14. Also, the microwave absorber terminations were always adjusted for maximum power transfer from the coaxial line circuits to the cavity circuit. This position varied from 1.385 cm to 1.623 cm from the cavity midplane for the .150" and .300" cavity heights, respectively. For the measurements where the center probe was shorted, a shorting plunger was adjusted inward until its end was flush with the cavity top wall, thus removing any input at the cavity center.

Microwave Absorber Load Test Circuit. Before making an external impedance measurement at one of the coaxial lines, it was desirable to measure the impedance of the microwave absorber terminating each coaxial line and to compare the measured results with calculated results. To do this, a test circuit which consisted of a .250" semi-rigid coaxial line and a .141" coaxial air line terminated with an adjustable microwave absorber, which was similar to the microwave absorber circuit in the test combiner, was fabricated. A cross section of this circuit is shown in Figure 15. A manual measurement of the microwave absorber impedance was made over the 9.1 to 10.48 GHz frequency range. As can be noted in Figure 16, the impedance of the microwave absorber load appears as the impedance of a transmission line with a characteristic impedance determined by the ECCOSORB material. The calculated impedance response is obtained using equations (20-24) and is shown as the dashed curve in Figure 16. A subroutine

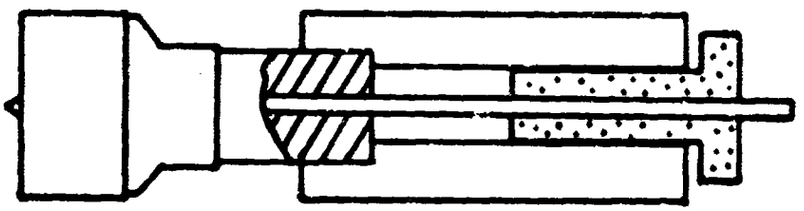

Figure 15. Microwave Absorber Load Test Circuit

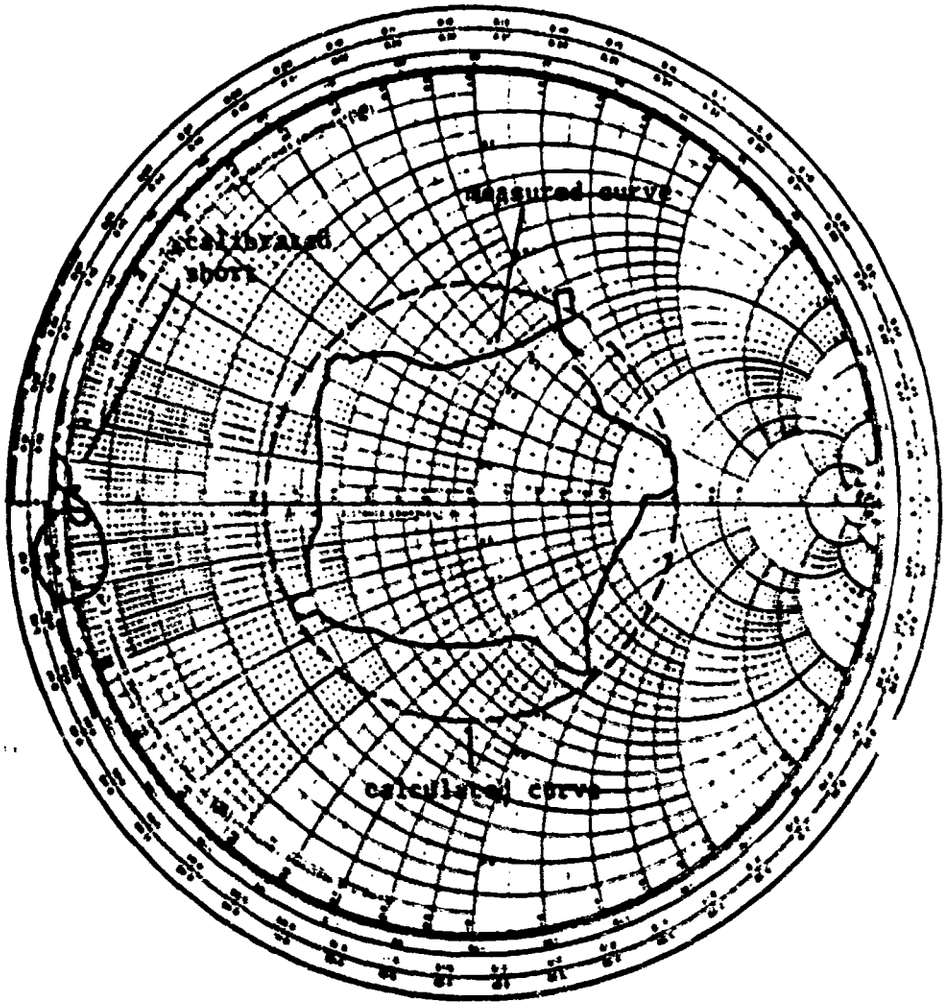


Figure 16. Microwave Absorber Measured versus Calculated Load Impedance, x=10.5 cm

of the ZCOMB program was used to calculate the microwave absorber impedance versus frequency. These two curves are quite similar in shape and both have approximately the same reference plane. The slight difference between the calculated and measured impedances is attributable to the use of permittivity and permeability constants which were measured at 8.6 GHz. Thus, the equations used to model the impedance response of the microwave absorber terminations are fairly accurate. To arrive at the calculated curve, the following data was used.

| | | |
|---|---|---|
| $\epsilon_r'$=16.2 F/m | $\mu_r'$=1.6 H/m | $\alpha$=21 dB/cm |
| $\epsilon_r''$=1.134 F/m | $\mu_r''$=.752 H/m | x=10.5 cm |

The values for the coefficients of the complex permittivity and permeability constants were measured by the manufacturer of ECCOSORB MF 116. The value x is the length of coaxial air line between the ANA reference plane and the microwave absorber, and $\alpha$ is the attenuation constant for MF 116. Using equation (25) and the quantities given above, $\alpha$ is calcualted to be 21.1 dB/cm at 8.6 GHz which compares favorably with the value given by the manufacturer.

Coaxial Line Impedance with the Center Probe Terminated in 50 ohms. These measurements are graphically shown in Figures 17 to 20 and consist of characterizing the impedance response of a single coaxial line with either all coaxial lines present or only the measured line present and with cavity heights of .150" and .300". The general equivalent circuit representation for this case is shown in Figure 8 and the defining equation to be referenced is (12). When all other coaxial lines are removed, the equivalent circuit must be modified to

show only one output line and the constant N in equation (12) must be set to one. By disregarding the resonant loops shown in these figures, the impedance is seen to be only the impedance of the microwave absorber as shown in Figure 17. Thus, the test circuit used for the microwave absorber impedance was representative of the circuit in the test combiner. The effect on the impedance of a single line caused by coupling RF power into the other coaxial lines is best shown in Figure 19 versus Figure 20 where the cavity height is .300". The result is that the $TM_{020}$ and $TM_{210}$ modes which are critically coupled and greatly overcoupled, respectively, in Figure 19 have their coupling reduced significantly. The $TM_{020}$ resonant frequency also changes significantly being reduced from 9.94 GHz to 9.775 GHz. This occurs somewhat because the effective cavity diameter is reduced with the addition of all the center conductors. The $TM_{210}$ mode, previously much overcoupled, actually is closer to being critically coupled at its resonant frequency than the $TM_{020}$ mode is. From equation (12), one would expect the coupling of the $TM_{020}$ mode to improve as N was increased, however, the unloaded Q and the external Q in this equation decrease rapidly causing the impedance at resonance to decrease also and giving the cavity response the appearance of a small resonant loop. With the coupling to the cavity being undercoupled, a large portion of the RF power from the source (i.e. a swept RF source or IMPATT diode) is absorbed into the microwave absorber termination. To achieve maximum combining efficiency, the circuit design will have to be such that the coupling of N lines to a cavity does not prevent critical coupling of each coaxial line. This will also more than likely keep the $TM_{210}$

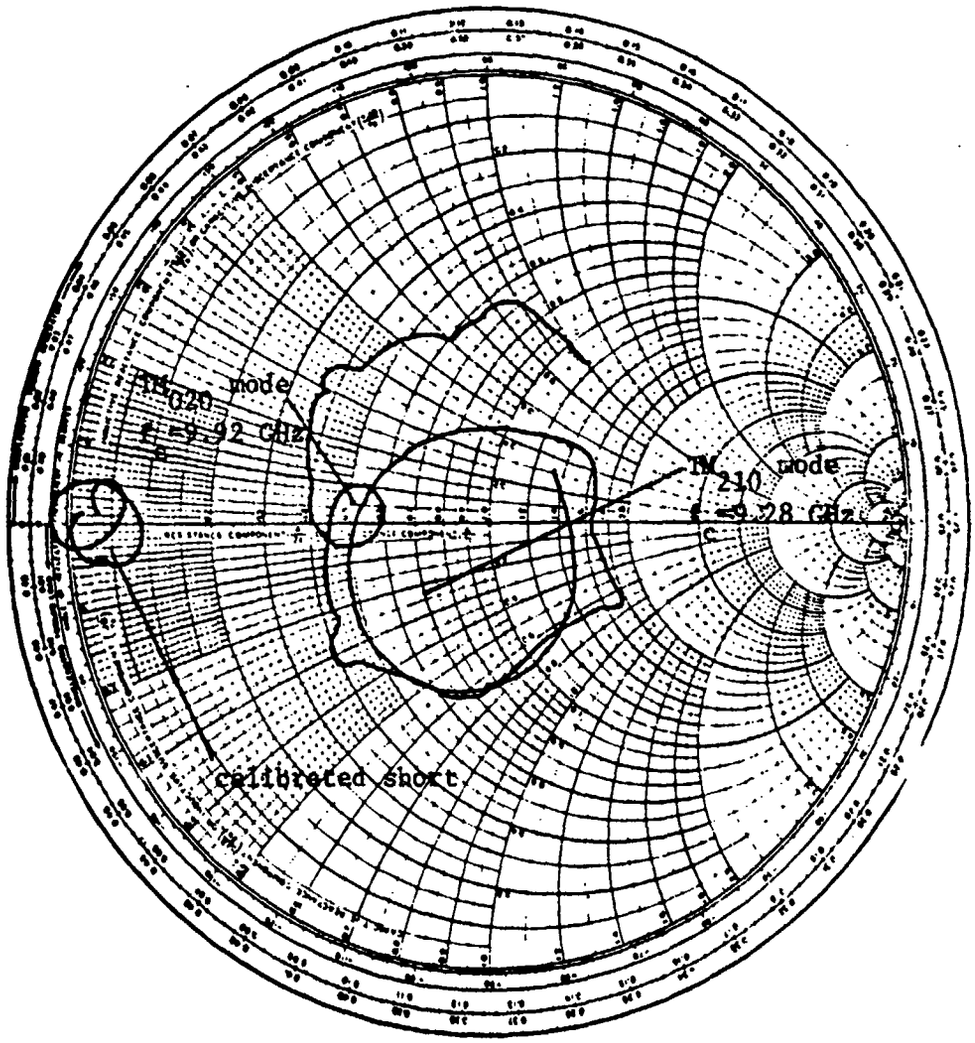


Figure 17. Coaxial Line Impedance, one line present, 50 ohm input, d=.150"

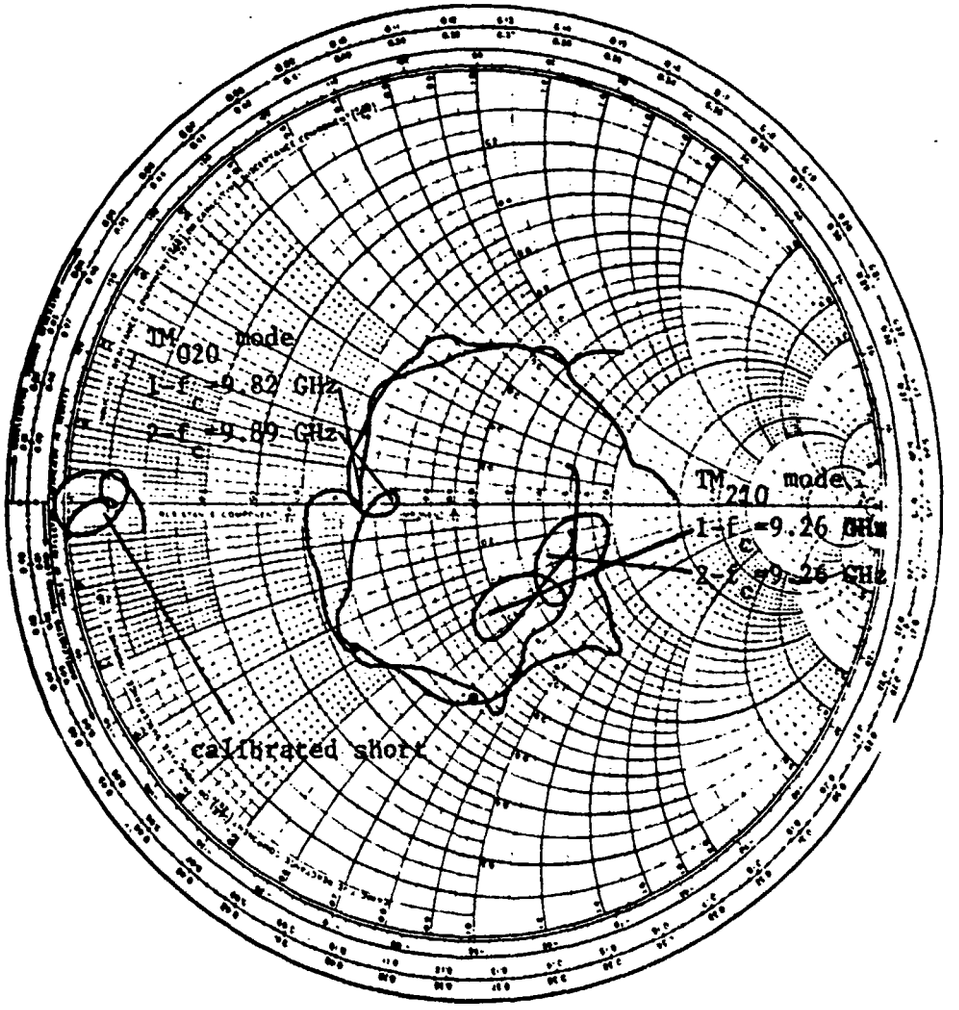


Figure 18. Coaxial Line Impedance, four lines present, 50 ohm input, d=.150". Case 1-input critically coupled. Case 2-input slightly undercoupled (ρ=.2).

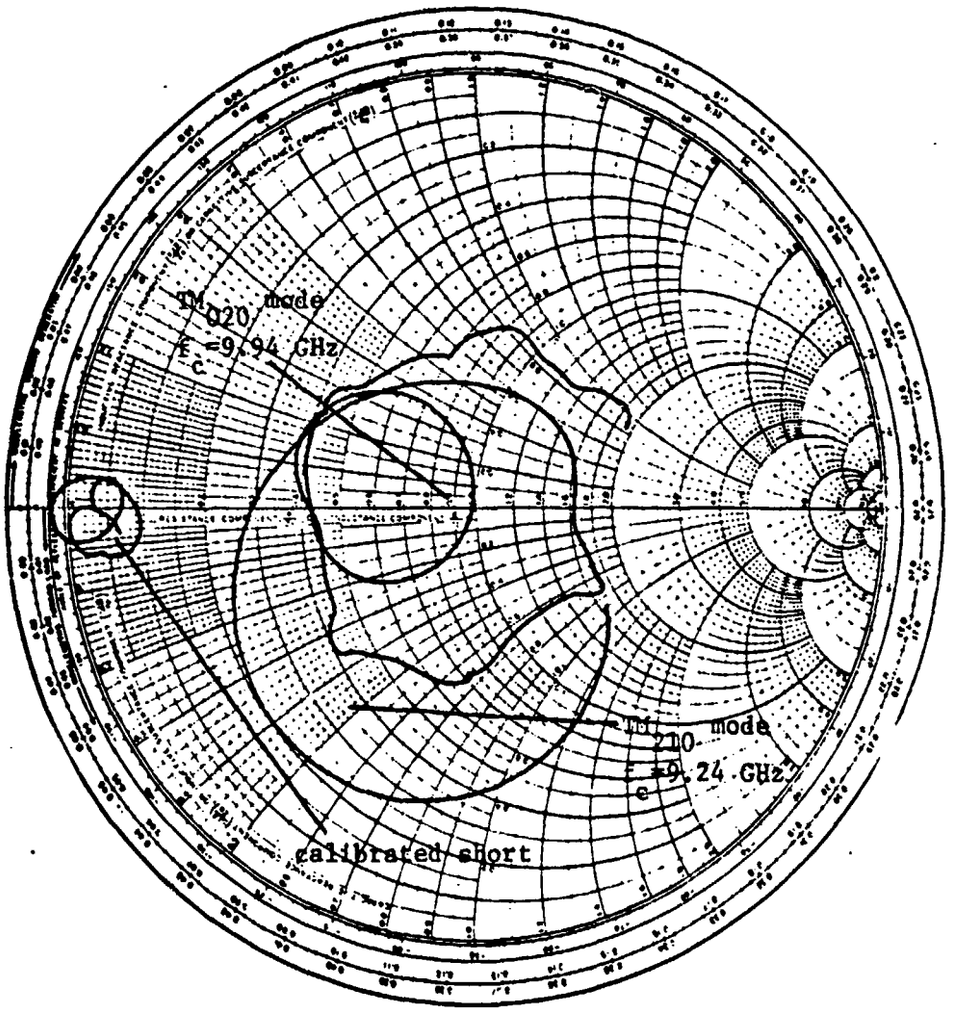


**Figure 19. Coaxial Line Impedance, one line present, 50 ohm input, d=.300"**

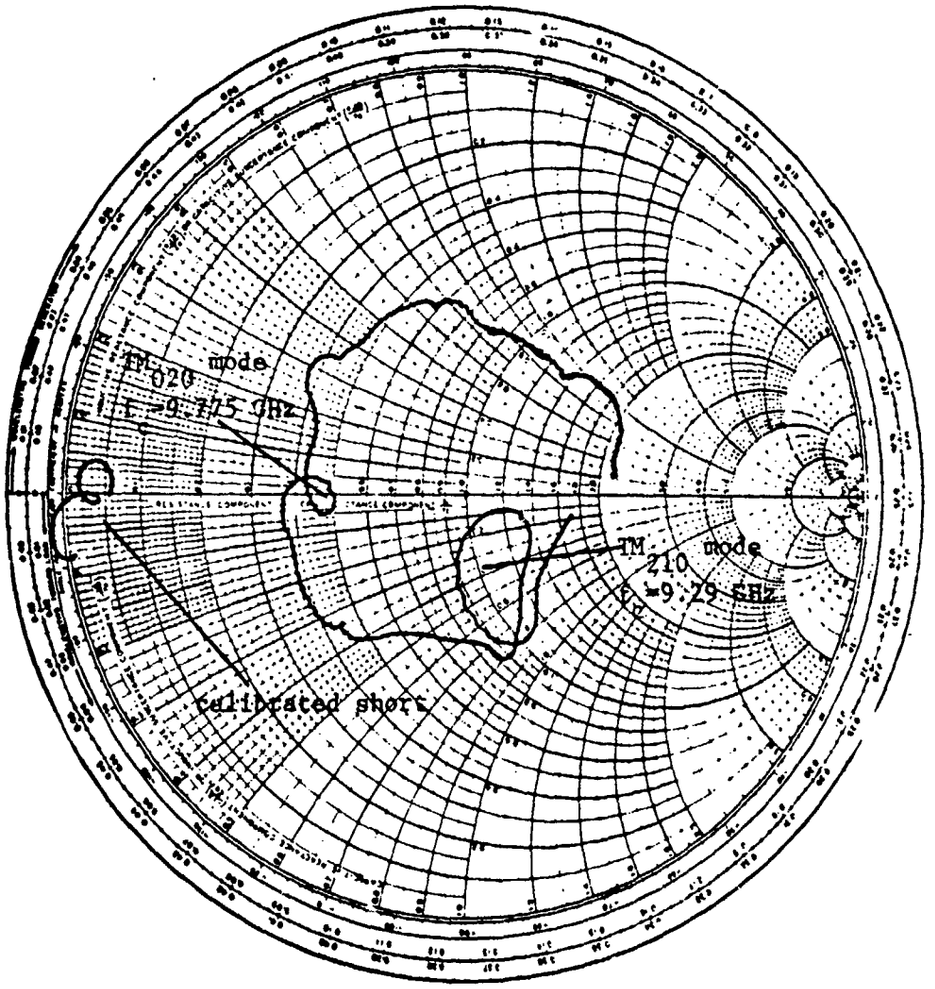


**Figure 20. Coaxial Line Impedance, four lines present, 50 ohm input, d=.300"**

mode overcoupled which is desirable for single mode operation. Figures 17 & 19 and 18 & 20 show the effect of changing the cavity height. Decreasing the cavity height does not appear to affect the $TM_{020}$ and $TM_{210}$ resonant frequencies but does appear to moderately affect the coupling of the coaxial line to the cavity. A decrease in cavity height causes a decrease in unloaded circuit Q as can be seen from equation (5) or Table 3 and subsequently the impedance response decreases. In the measurement of coaxial line impedance with four lines present, a 50 ohm input, and a cavity height of .150" (Figure 18), the resonant cavity response was nearly eliminated with the center probe being critically coupled. However, the cavity response was restored when the center probe was slightly undercoupled.

Coaxial Line Impedance with the Center Probe Short Circuited. These measurements were performed to demonstrate the effect the input circuit has on the impedance matching of the coaxial lines to the cavity. By short circuiting the combiner input probe, the external load and ideal transformer representing input coupling in the equivalent circuit is removed from considerstion as shown in Figure 21. Again, measurements were made with and without coaxial lines at two different cavity heights. The impedance responses are provided in Figures 22 to 25. With a cavity height of .150" and only one coaxial line, the coupling shown in Figure 22 to the cavity $TM_{020}$ mode is critical while the $TM_{210}$ mode coupling is overcoupled. Adding the other lines to the circuit again undercouples the coaxial lines to the $TM_{020}$ and $TM_{210}$ modes as seen in Figure 23. However, the change in coupling is not quite as great as when the external input load is

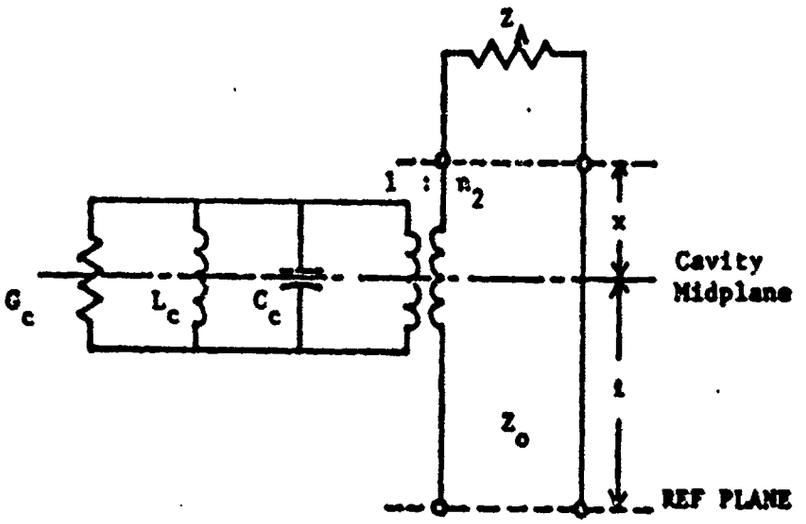


Figure 21. Equivalent Circuit of a $TM_{020}$ Combiner with the Cavity Probe Short Circuited and One Coaxial Line Present

present. The resonant frequency for the $TM_{020}$ and $TM_{210}$ modes is approximately 9.92 GHz and 9.25 GHz, respectively, and is not affected by the addition or deletion of coaxial lines. Since the resonant frequencies are a function of the cavity radius, the addition of the coaxial lines affects the cavity radius minimally for this test combiner. This is not necessarily true in larger power combiners, however, where many coaxial lines would be present. Both the $TM_{020}$ and $TM_{210}$ modes are overcoupled as shown in Figure 24 (i.e. most of the RF power is absorbed into the cavity walls) for the case of one coaxial line and a cavity height of .300". Comparison of this figure with Figure 19 where the input is not shorted, demonstrates the relative effect the external load has on the loaded Q of the circuit. The difference in the $TM_{020}$ response is small while the $TM_{210}$ response changes moderately. This indicates that the external circuit impedance (usually 50 ohms) has more of a shunting effect on the $TM_{210}$ mode. Including the coaxial lines to the short circuited, .300" high cavity again reduces the coaxial to resonant mode coupling but the reduction is much less than when a 50 ohm input is used. The impedance data so far indicates that the external load has a moderate effect on the impedance at a single coaxial line while addition of the other lines affects the impedance response significantly because of the net low impedance shunting the cavity. As described in the previous case, changing the cavity height does not affect the $TM_{020}$ and $TM_{210}$ resonant frequencies to any great extent.

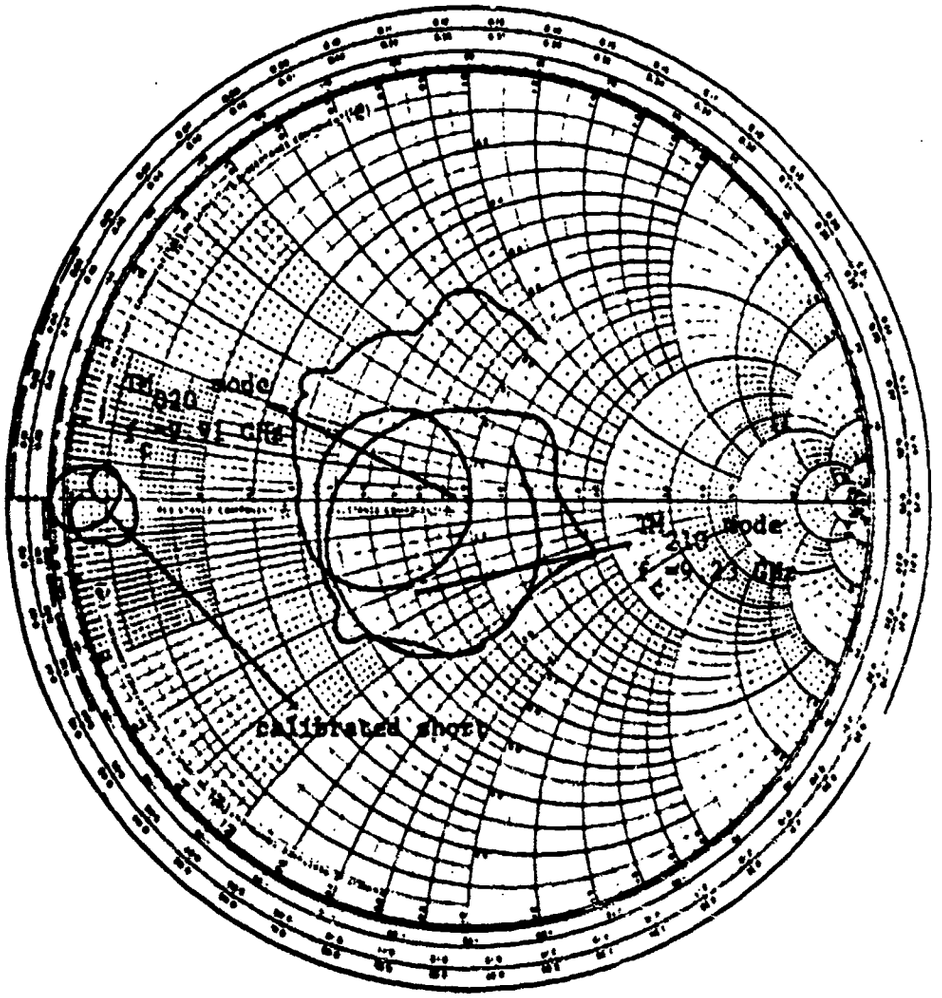


Figure 22. Coaxial Line Impedance, one line present, input shorted, d=.150"

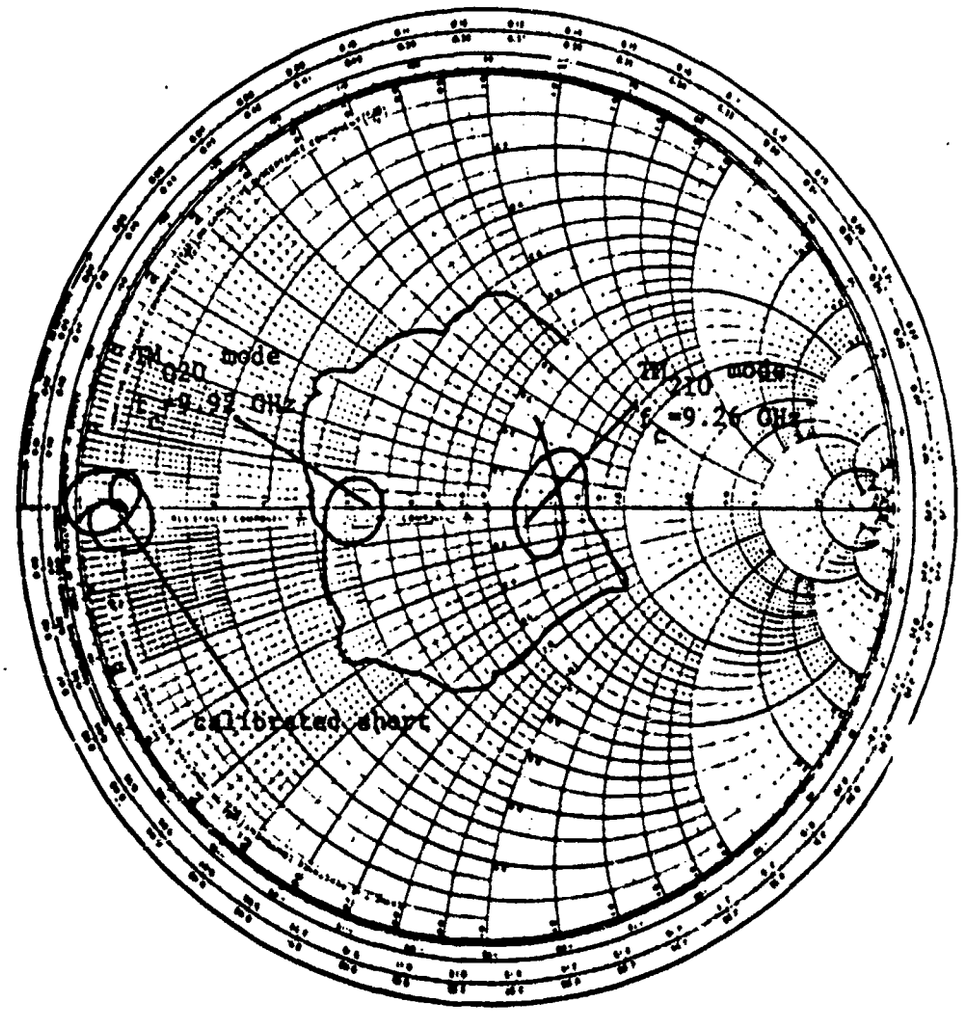


**Figure 23. Coaxial Line Impedance, four lines present, input shorted, d=.150"**

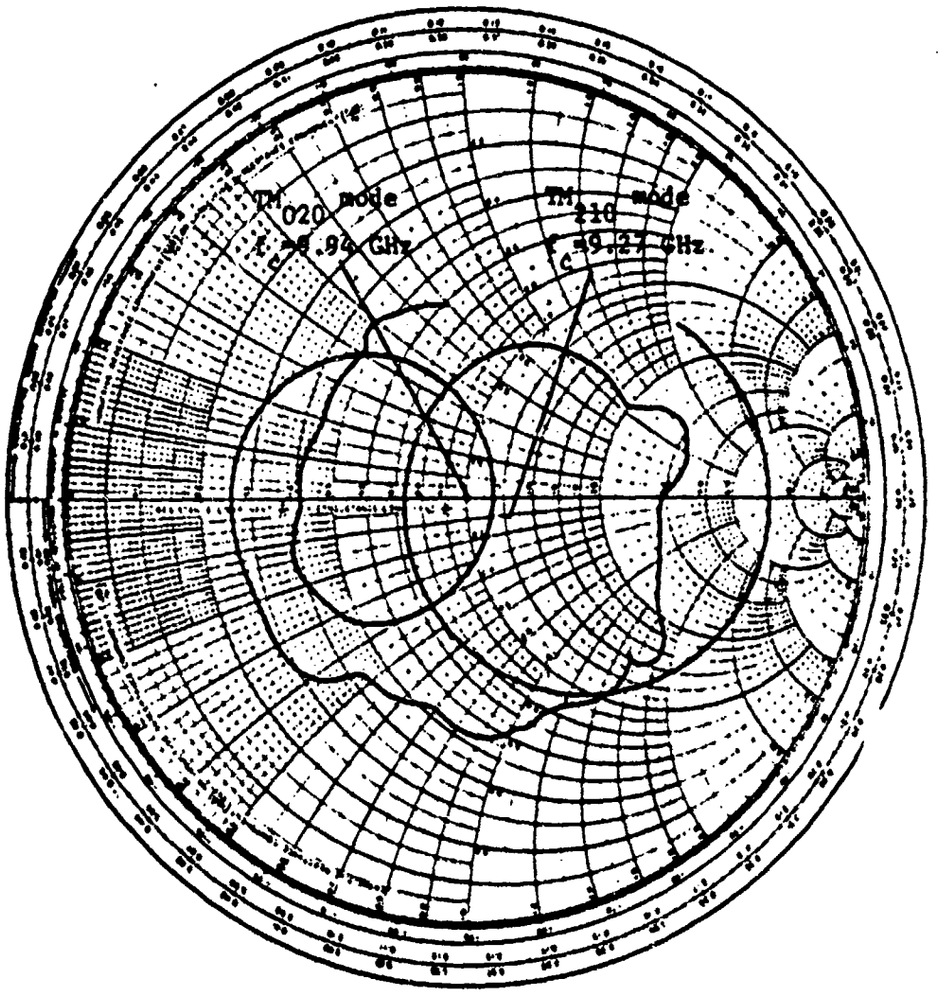


Figure 24. Coaxial Line Impedance, one line present, input shorted, d=.300"

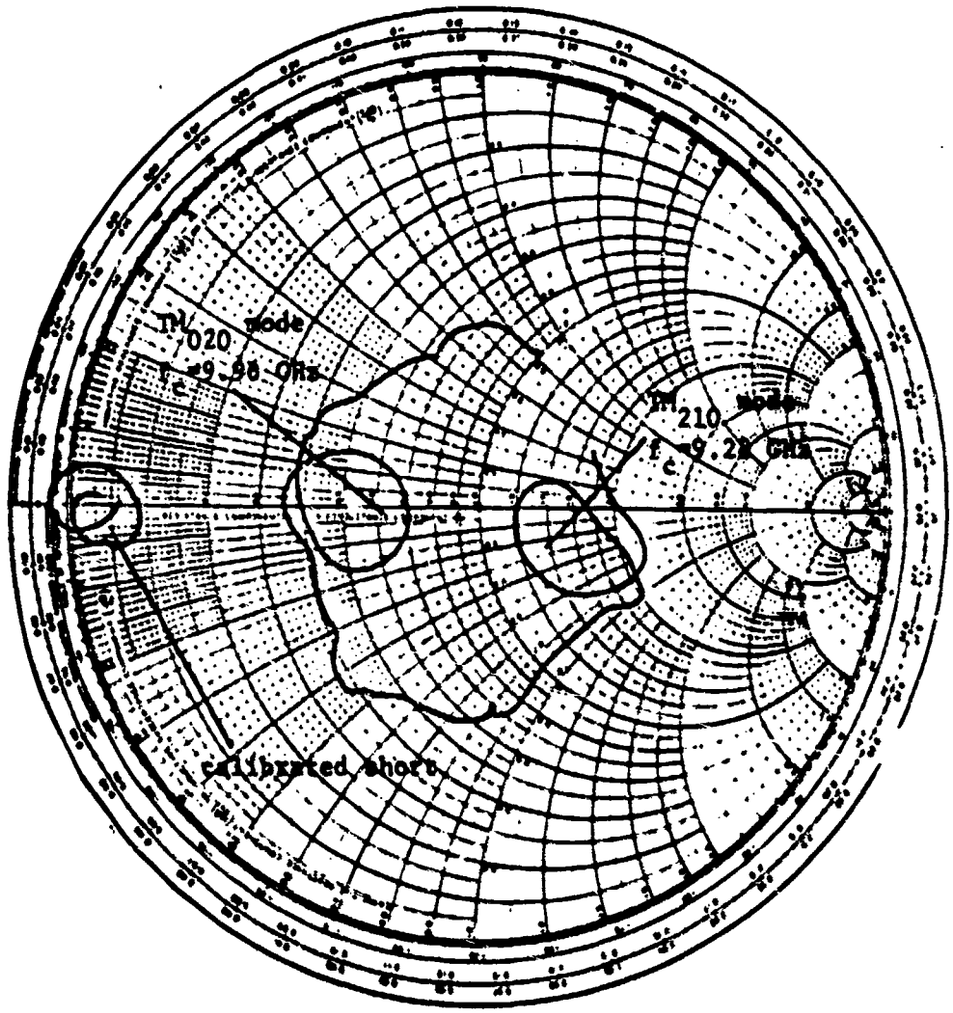


Figure 25. Coaxial Line Impedance, four lines present, input shorted, d=.300"

## Transmission Measurements

Two types of transmission measurements were performed. They were comprised of measuring the transmission of RF power from the combiner center probe to one of the coaxial lines and measuring the coaxial line-to-line transmission (isolation) properties. The first measurement provides information on the combining efficiency of the circuit and the second provides information on the isolation between lines. The measurements were made using the ANA in the transmission mode. The measured frequency range was 9.0 to 10.5 GHz.

Center Probe to Coaxial Line Transmission. The transmission coefficient of the test combiner in this configuration was measured with only one coaxial line present. Only one line was used because an external combining network was not available. The transmission measurements as shown in Figures 26 and 27 were made using cavity heights of .150" and .300". The input center probe and the microwave absorber load positons were adjusted to give the best coupling to the $TM_{020}$ mode possible. In the measurement, the center probe position had little effect on combining efficiency while the microwave absorber load position had a significant effect. This indicated that the combining efficiency is primarily determined by the coupling of RF power from the coaxial line to the cavity. In general, the transmission measurements of the test combiner indicated a higher than expected transmission loss. For the .150" and .300" high cavities the transmission loss was 6 dB and 3 dB, respectively, which relates to a 25% and 50% combining efficiency. The loss that occurs is attributable to the cavity wall loss, to the spacing of the coaxial line center con-

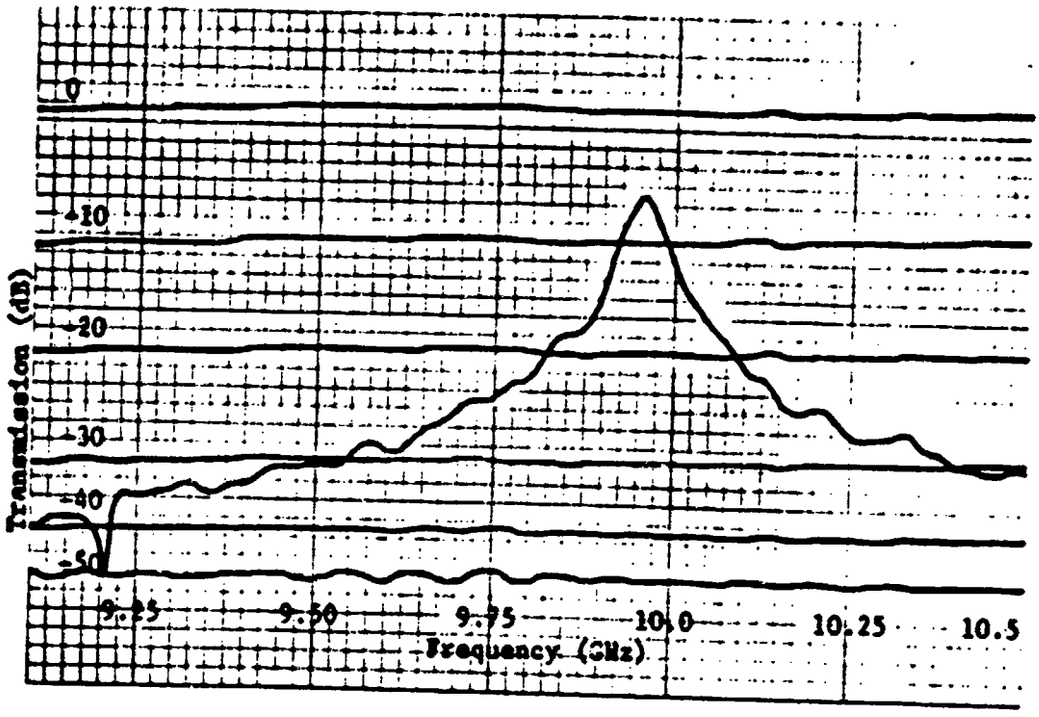


Figure 26. Center Probe to Coaxial Line Transmission, d=.150"

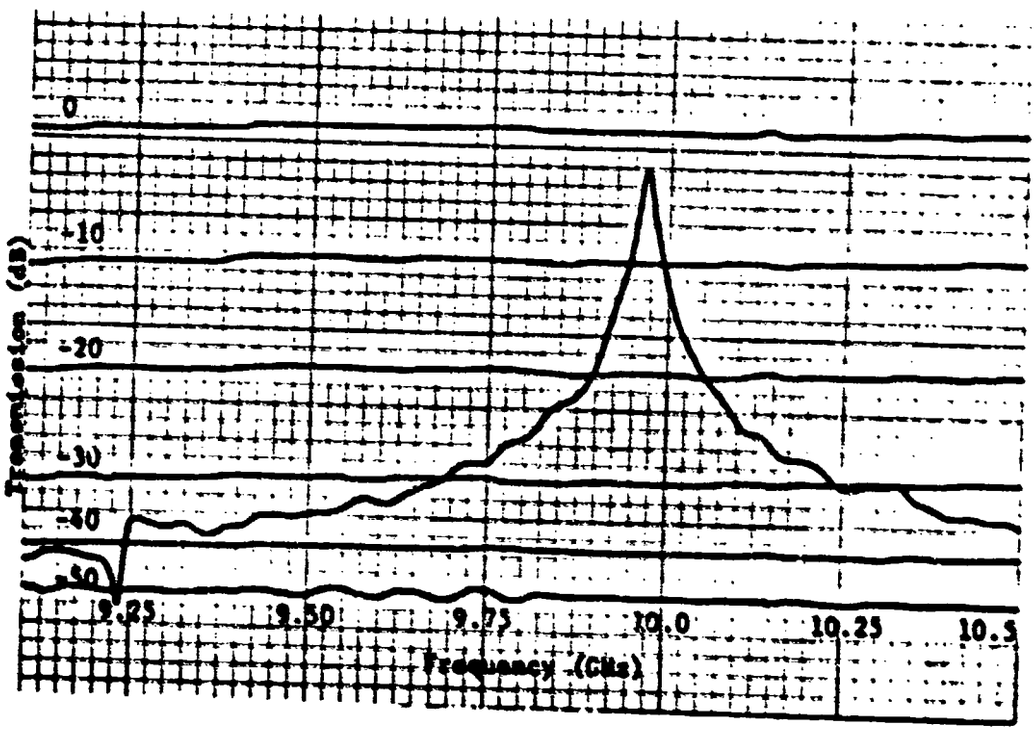


Figure 27. Center Probe to Coaxial Line Transmission, d=.300"

ductor with respect to the cavity wall, and to the loss of power into the microwave absorber. There is also approximately .5 dB loss which occurs at the transition from the combiner coaxial air line to the semi-rigid coaxial line used to connect the test combiner to the ANA. As the coaxial line center conductor is moved radially inward, the coupling to the cavity, and hence combining efficiency, will increase, but the isolation between diode circuits will decrease. The impedance of the microwave absorber can also control efficiency with a load representing a short circuit producing the best efficiency. However, as stated by Kurokawa a short circuit presented to an IMPATT diode can lead to instability. In general, the circuit impedance presented to an IMPATT diode should always be greater than or equal to its negative real part. A compromise between a short circuit impedance and the impedance presented by ECCOSORB MF 116 or any other microwave absorber should be possible and would improve current efficiency potential of $TM_{ono}$ combiners. To achieve a lower impedance as suggested, a $\lambda/4$ transformer could be used between the microwave absorber and the cavity.

Coaxial Line-to-Line Isolation. This measurement was comprised of measuring the transmission loss between two adjacent coaxial lines of the test combiner with a .300" high cavity. One measurement was made with the center probe short circuited (Figure 28) and another was made with the center probe terminated in a 50 ohm impedance (Figure 29). The worst case isolation measurement shown in Figure 28 occurs with the center probe short circuited. This figure indicates a 10 dB and 9 dB isolation for the $TM_{210}$ and $TM_{020}$ modes, respectively. When the input

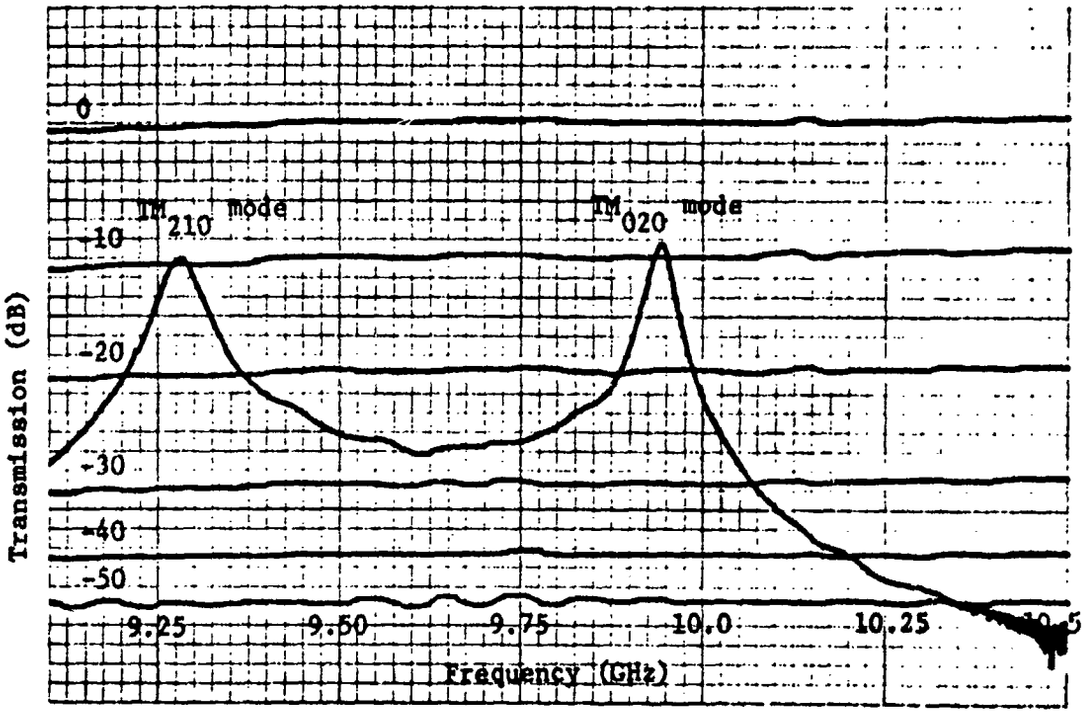


Figure 28. Coaxial Line-to-Line Isolation, input shorted, d=.300"

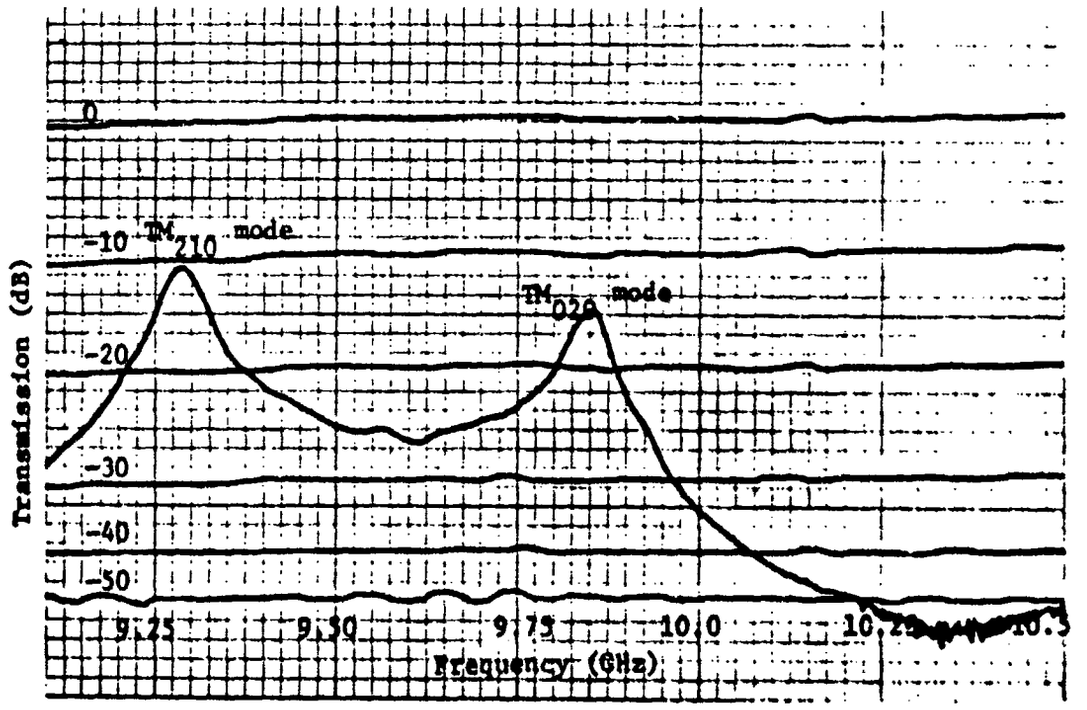


Figure 29. Coaxial Line-to-Line Isolation, 50 ohm input, d=.300"

is terminated in 50 ohms, the isolation for the $TM_{210}$ mode remains approximately the same, but for the $TM_{020}$ mode, the isolation improves to 15 dB. Another effect the 50 ohm input had on the $TM_{020}$ mode was to shift its resonant frequency downward from 9.94 GHz to 9.85 GHz while the $TM_{210}$ resonant frequency stayed constant at 9.29 GHz. This frequency shift could have occurred as the result of a slight perturbation of the center probe below the cavity top wall. The isolation performance between each of the coaxial lines is relatively good as expected.

## Correlation of Measured and Calculted Results

In this section, the calculated impedance response for only the $TM_{020}$ mode of a single coaxial line and then all four lines is presented and compared to the measured responses shown earlier. To calculate the coaxial line impedance response, a program called Z COMB was used and is described in Appendix A. Only the $TM_{020}$ response was calculated because of limited calculator memory. This program is based upon Kurokawa's model but unlike his model, it uses equations (20-24) to describe the microwave absorber impedance. Two unknowns in the model which had to be determined were the coupling coefficients $n_1^2$ and $n_2^2$ whose values were approximated as $8.41 \times 10^{-4}$ and $6.5 \times 10^{-4}$, respectively. The value of $n_1^2$ was approximated with the equation $n_1^2 = G_c/Z_o$ (i.e. because $G_c$ is not accurately known as a result of the scallops) when the input coupling coefficient $\beta_1$ is equal to one. The value of $n_2^2$ was approximated by fitting the calculated curve to the measured data for the case of a single coaxial line. The reference planes for

the position of the microwave absorber and for calculating the impedance looking into a coaxial line also had to be chosen. These distances were chosen as 1.5 cm and 10.5 cm, respectively, which were approximately the same as used in the coaxial line impedance measurements. The calculated impedance response of a single coaxial line with no other lines present and with a cavity height of .300" is shown in Figure 30. The response is critically coupled at the $TM_{020}$ resonant frequency (i.e. 10 GHz) and has a characteristic impedance equal to $Z_A$ away from resonance. The calculated response shown compares favorably with the measured response, using the same parameters, shown in Figure 19. By referring to equation (12), it can be noted that the coaxial line impedance should increase and become overcoupled as the number of coaxial lines increases assuming no change in loaded Q. In the measured result of Figure 20 where the number of lines was increased from one to four, the impedance response became significantly undercoupled. To account for this in the calculator model, a new value of $.406 \times 10^{-4}$ was selected for the coupling coefficient $n_2^2$. The impedance response with this value, shown in Figure 31, is very similar to that of the measured result of Figure 20. To explain this discrepancy it is suggested that even though the number of coaxial lines is increasing, the the loaded cavity Q also decreases with the addition of coaxial lines and thus, has a more predominant effect on coaxial line impedance than the value N. This is substantiated by the measured results which indicated that lowering the cavity Q did affect the impedance response of the combiner network significantly.

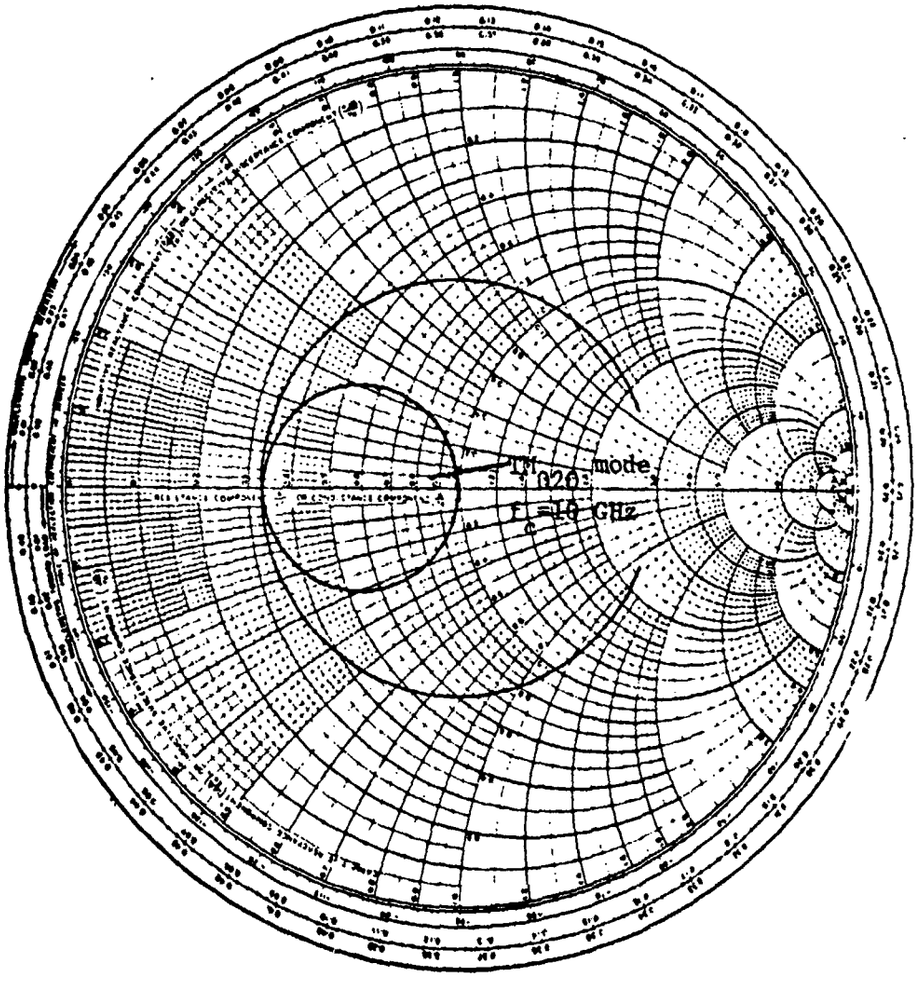


Figure 30. Calculated Coaxial Line Impedance Response, one coaxial line, d=.300", $n_2^2$=6.5 X $10^{-4}$

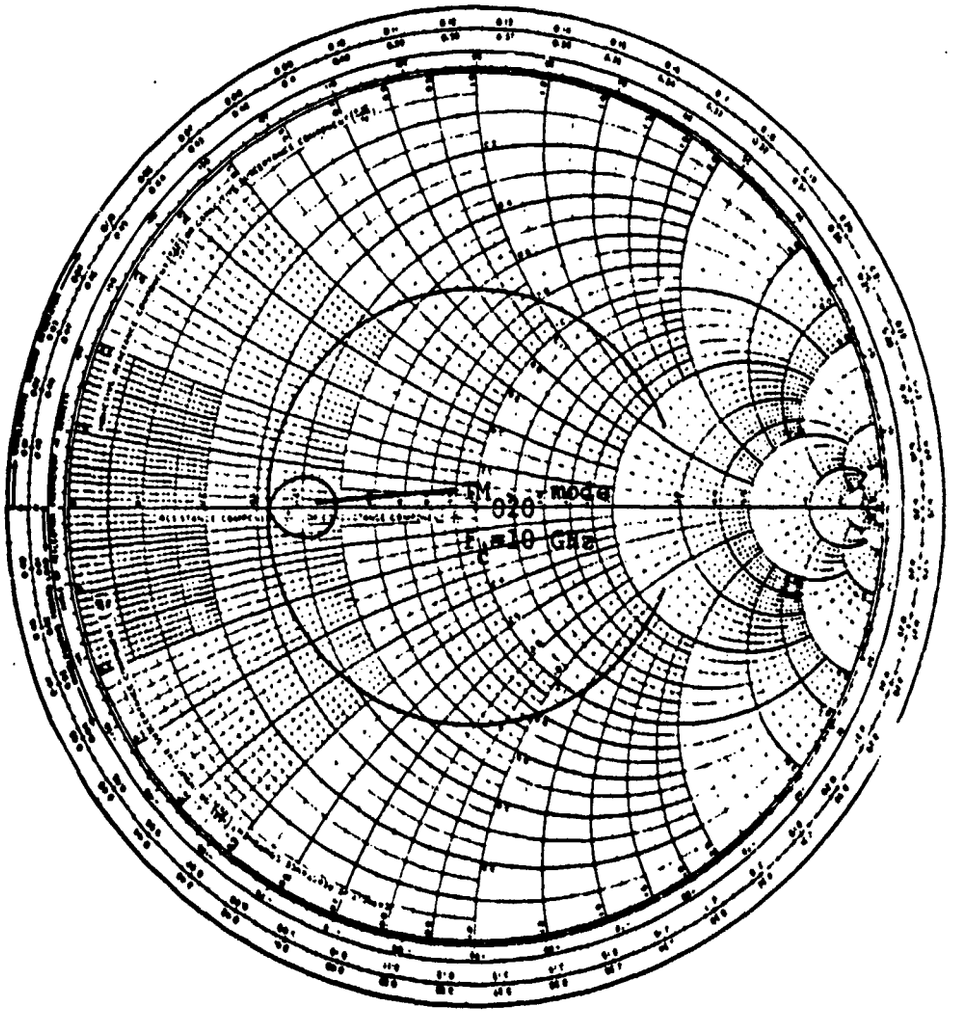


Figure 31. Calculated Coaxial Line Impedance Response, four lines present, d=.300", $n_2^2 = .406 \times 10^{-4}$

## CHAPTER V

## SUMMARY AND CONCLUSIONS

As stated in the introduction, the objective of this investigation has been directed toward increasing the understanding of $TM_{ono}$ combiner design. In particular, a more accurate model of the impedance presented to an IMPATT diode was of interest. Toward this goal, the theory of cylindrical resonant cavity combiners, the circuit modelling of resonant cavity combiners, and the characterization of a $TM_{020}$ test combiner was presented. The general theory of cylindrical resonant cavities and the coaxial diode circuits is fairly well understood as is shown by the design equations presented and the characterization of the $TM_{020}$ test combiner. The Kurokawa model was presented and used as the basic model for describing the impedance of the combiner network presented to the IMPATT diode circuit. By comparing the measured versus calculated coaxial line impedance responses in chapter IV, it can readily be seen that this model does for the most part provide the intrinsic response of the $TM_{ono}$ combiner. To achieve this response, however, the coupling coefficients were approximated in order to fit the calculated curves to the measured data. Additionally, when the number of coaxial lines was increased from one to four, a smaller value of the cavity/coaxial line coupling coefficient was required to again fit the curve. Thus, it is apparent that there exists

more than a simple relationship between the coaxial line impedance response and the number of coaxial lines. In fact, because the additional lines cause a significant reduction in loaded Q of the combiner, the Kurokawa model needs to be modified to include the changes in Q and coupling coefficient, $n_2^2$. Further comparison between measured and calculated data is needed to accurately determine the functional dependence of this relationship.

Another very important factor in the design of $TM_{ono}$ combiners is achieving the highest combining efficiency possible. Achieving high combining efficiency is synonomous with obtaining maximum power transfer from the coaxial line circuits to the cavity and vice versa. To obtain maximum power transfer, both mismatch and dissipative losses for the cavity/coaxial line interface must be minimized. The mismatch losses are minimized by critically coupling the coaxial line impedance to the cavity impedance at resonance. Because the number of coaxial lines and the cavity height significantly affects this coupling (i.e. through reduction in cavity Q), the design of $TM_{ono}$ combiners must incorporate design rules which will maintain high cavity Q for any size combiner. Generally, any perturbation (e.g. probes, loops, coaxial lines) of a resonant cavity increases the loss and decreases the Q of the resonant circuit under consideration with smaller perturbations affecting the Q of a resonant circuit less. Thus, it is concluded that the use of smaller coaxial lines would be beneficial in improving combining efficiency. The dissipative loss in a $TM_{ono}$ combiner includes loss in the cavity walls and loss in the microwave absorber. With respect to the wall loss, the scalloped

contours for the coaxial lines causes the majority of this loss. To reduce the wall loss, the coaxial line may be moved closer to the cavity with some sacrifice in isolation between diode circuits. There is also a finite loss in the microwave absorber load and this loss may be reduced as stated earlier by decreasing the characteristic impedance (e.g. using $\lambda/4$ transformers) in front of the absorber. The microwave absorber impedance cannot be reduced too much, however, because of IMPATT diode stability considerations.

In summary additional experiments are needed in which the physical and electrical parameters of the cavity/coaxial line interface, as mentioned above, are varied in order to determine the relationship between the combiner Q, the coupling coefficient $n_2^2$, and the number of diode circuits and also in order to optimize the combining efficiency. Furthermore, even though it was not emphasized, the model of a $TM_{onc}$ combiner should be extended to include possible IMPATT diode interaction with nonsymmetrical modes. No new combiner models were developed in this investigation. However, this investigation has delineated some very important aspects of $TM_{onc}$ combiner design.

## APPENDIX A

### ZCOMB Program

This program was developed to calculate the impedance, $Z'_N$, as a function of frequency at a single coaxial line of a $TM_{ono}$ resonant combiner. The impedance can be calculated at any convenient reference plane relative to the cavity midplane. The program is based on the Kurokawa combiner model. Equation (12) was rearranged into the following form for easier implementation in the calculator routine.

$$Z_N = Z_A + \frac{j\frac{ff_c N \eta_2^2}{Q_e G_e}}{(f_c^2 - f^2) + j\frac{ff_c}{Q_e}\left(1 + \frac{\eta_L^2}{Z_o G_e}\right)} \qquad (28)$$

The microwave absorber load impedance is computed in a subroutine of this program and uses equations (20-24). The impedance, $Z'_N$, is computed using an additional calculator program called IN Z (Appendix B) which calculates the input impedance to a length of loaded transmission line. A flow chart of the ZCOMB program is provided in Figure 32 and a listing of the program is given in Table 4. The programs ZCOMB and IN Z are implemented in HP's Reverse Polish Notation language for use on the HP 41C programmable calculator. To run the program, it is called from memory and the $TM_{ono}$ combiner parameters are entered into registers 0-32 and the X&Y stack registers. A listing of the register inputs is provided in Table 5. The start, stop, and step frequencies in MHz are next entered and individual data points of $Z'_N$ are calculated as a function of frequency with each run.

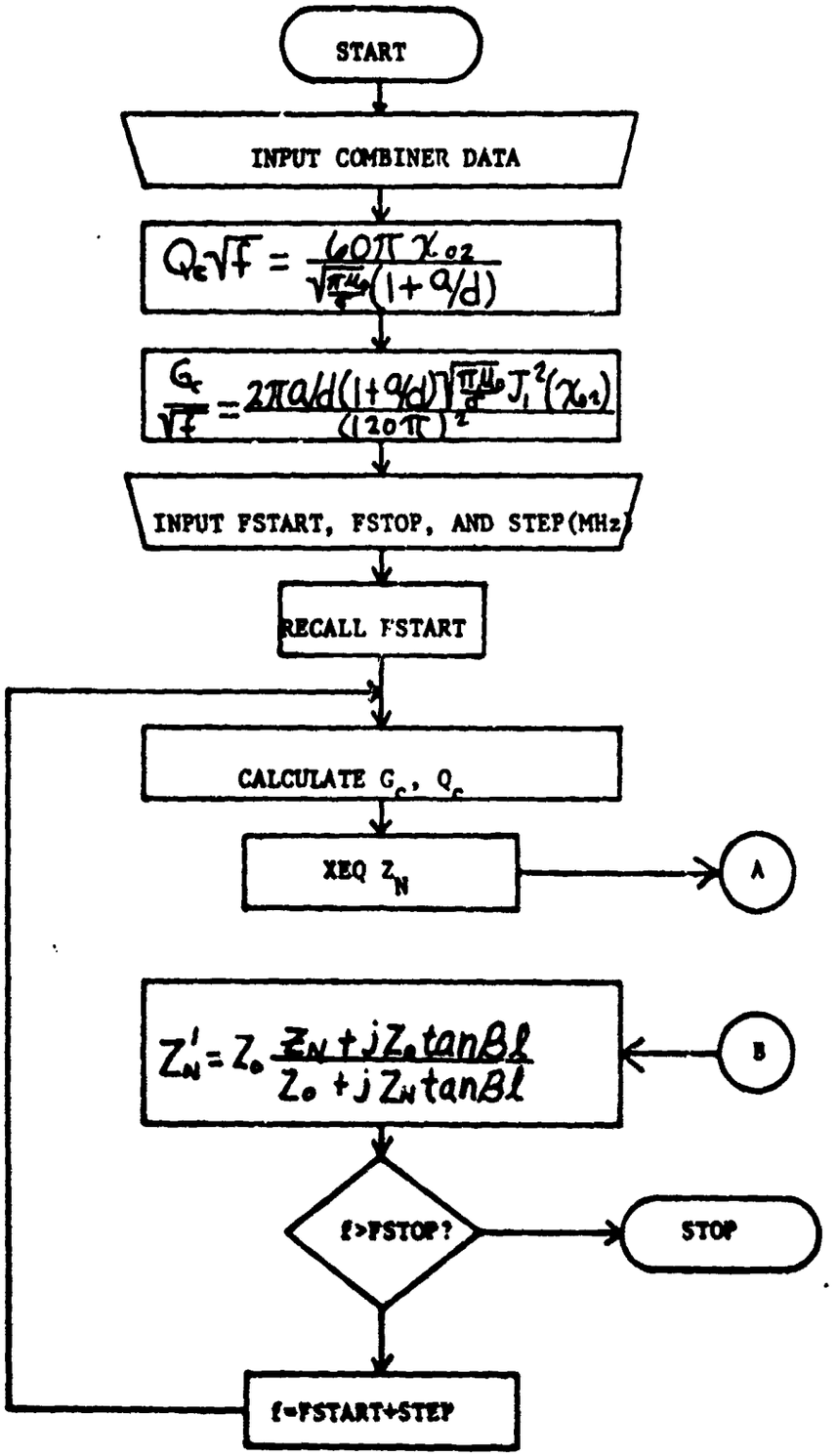


Figure 32. Flowchart of ZCOMB program

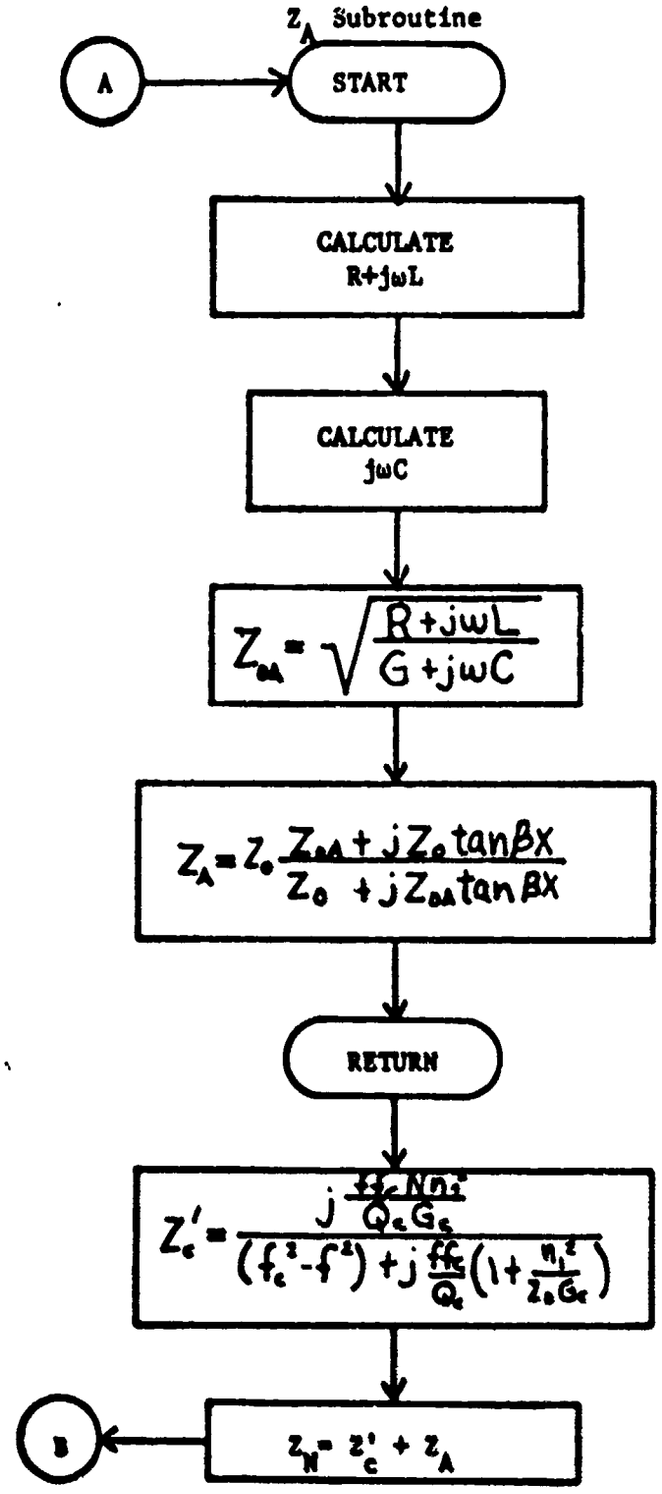


Figure 32(con't).

TABLE 4. ZCOMB Program Listing

| Address | Key | Comment | Address | Key | Comment |
|---|---|---|---|---|---|
| 01 | LBL ZCOMB | | 46 | RCL 31 | |
| 02 | INPUT DATA | | 47 | / | $Q_c$ |
| 03 | AVIEW | | 48 | STO 26 | |
| 04 | STOP | | 49 | XEQ ZA | |
| 05 | / | | 50 | CLST | |
| 06 | STO 00 | | 51 | RCL 27 | |
| 07 | 1 | | 52 | 1/X | |
| 08 | + | | 53 | STO 30 | |
| 09 | STO * 00 | | 54 | RCL 11 | |
| 10 | 1/X | | 55 | * | |
| 11 | STO 22 | | 56 | .02 | |
| 12 | RCL 10 | | 57 | * | |
| 13 | STO * 00 | | 58 | 1 | |
| 14 | STO / 22 | | 59 | + | |
| 15 | PI | | 60 | STO 29 | |
| 16 | STO + X | | 61 | RCL 12 | |
| 17 | STO * 00 | | 62 | STO * 30 | |
| 18 | 30 | | 63 | RCL 26 | |
| 19 | * | | 64 | STO / 29 | |
| 20 | STO * 22 | | 65 | STO / 30 | |
| 21 | STO + X | | 66 | RCL 15 | |
| 22 | $X^2$ | | 67 | STO * 29 | |
| 23 | STO / 00 | | 68 | STO * 30 | |
| 24 | RCL 09 | | 69 | $X^2$ | |
| 25 | STO * 22 | | 70 | RCL 23 | |
| 26 | RCL 14 | | 71 | STO * 29 | |
| 27 | $X^2$ | | 72 | STO * 30 | |
| 28 | STO * 00 | | 73 | $X^2$ | |
| 29 | FSTART=? | (MHz) | 74 | - | |
| 30 | PROMPT | | 75 | RCL 29 | |
| 31 | STO 23 | | 76 | $X \leftrightarrow Y$ | |
| 32 | FSTOP=? | (MHz) | 77 | XEQ CPINV | |
| 33 | PROMPT | | 78 | RCL 30 | |
| 34 | STO 24 | | 79 | 0 | |
| 35 | STEP=? | (MHz) | 80 | XEQ CMULT | $Z'_c$ |
| 36 | PROMPT | | 81 | RCL 08 | |
| 37 | STO 25 | | 82 | RCL 07 | |
| 38 | LBL 01 | | 83 | XEQ CADD | $Z_M = Z_A + Z'_c$ |
| 39 | RCL 23 | RCL FSTART | 84 | STO 04 | |
| 40 | SQRT | | 85 | $X \leftrightarrow Y$ | |
| 41 | STO 31 | | 86 | STO 05 | |
| 42 | RCL 00 | | 87 | RCL 23 | |
| 43 | * | $G_c$ | 88 | RCL 32 | |
| 44 | STO 27 | | 89 | XEQ IN Z | $Z'_M$(Rect.) |
| 45 | RCL 22 | | 90 | R-P | |

TABLE 4(con't)

| Address | Key | Comment | Address | Key | Comment |
|---|---|---|---|---|---|
| 91 | 50 | | 136 | STO 05 | |
| 92 | / | | 137 | RCL 23 | |
| 93 | P-R | $Z'_N/Z_o$ | 138 | RCL 13 | |
| 94 | X= | | 139 | XEQ IN Z | $Z_A$(Rect.) |
| 95 | ARCL X | | 140 | RTN | |
| 96 | APPEND Y | | 141 | LBL 02 | |
| 97 | ARCL Y | | 142 | END | |
| 98 | AVIEW | | | | |
| 99 | TONE 6 | | | | |
| 100 | STOP | | | | |
| 101 | RCL 24 | | | | |
| 102 | RCL 23 | | | | |
| 103 | X > Y? | f FSTOP? | | | |
| 104 | GTO 02 | | | | |
| 105 | RCL 25 | | | | |
| 106 | STO + 23 | f=FSTART+STEP | | | |
| 107 | GTO 01 | | | | |
| 108 | LBL ZA | $Z_A$ subroutine | | | |
| 109 | RCL 17 | | | | |
| 110 | RCL 16 | | | | |
| 111 | RCL 31 | | | | |
| 112 | * | | | | |
| 113 | P-R | | | | |
| 114 | RCL 18 | | | | |
| 115 | RCL 23 | | | | |
| 116 | * | | | | |
| 117 | RCL 19 | | | | |
| 118 | $X^2Y$ | | | | |
| 119 | P-R | | | | |
| 120 | XEQ CADD | R+jωL | | | |
| 121 | R-P | | | | |
| 122 | RCL 20 | | | | |
| 123 | RCL 23 | | | | |
| 124 | * | $\lvert j\omega C \rvert$ | | | |
| 125 | / | | | | |
| 126 | RCL 19 | | | | |
| 127 | STO - Z | | | | |
| 128 | R↓ | | | | |
| 129 | SQRT | | | | |
| 130 | 2 | | | | |
| 131 | STO / Z | | | | |
| 132 | R↓ | $\lvert Z_{OA} \rvert$ | | | |
| 133 | P-R | | | | |
| 134 | STO 04 | | | | |
| 135 | $X^2Y$ | | | | |

TABLE 5. ZCOMB Program Register Listing

| Register | Data |
|---|---|
| X | Cavity height, d(in. or cm) |
| Y | Cavity radius, a(in. or cm) |
| 00 | † |
| 01 | † |
| 02 | † |
| 03 | Coaxial line characteristic impedance, $Z_o$=50 ohms |
| 04 | † |
| 05 | † |
| 06 | † |
| 07 | † |
| 08 | † |
| 09 | Bessel function ordered zero $X_{on}$ |
| 10 | $R_s/\sqrt{f}=3.218 \times 10^{-4}$ |
| 11 | Input coupling coefficient, $n_1^2$ |
| 12 | Output coupling coefficient, $n_2^2$ |
| 13 | Distance from cavity midplane to microwave absorber, x(cm) |
| 14 | $J_m(X_{mn})$ |
| 15 | Cavity center frequency, $f_c$(MHz) |
| 16 | $\lvert R/\sqrt{f}\rvert=.1209$ |
| 17 | $\angle R/\sqrt{f}=-12.59^\circ$ |
| 18 | $\lvert j\omega L/f\rvert=1.802$ |
| 19 | $\angle j\omega L/f=64.82^\circ$ |
| 20 | $\lvert j\omega C/f\rvert=6.996 \times 10^{-3}$ |
| 21 | $\angle j\omega C/f=86^\circ$ |
| 22 | † |
| 23 | Start frequency, FSTART(MHz) |
| 24 | Stop frequency, FSTOP(MHz) |
| 25 | Step frequency, STEP(MHz) |
| 26 | † |
| 27 | † |
| 28 | † |
| 29 | † |
| 30 | † |
| 31 | † |
| 32 | Distance from reference plane to cavity midplane, t(cm) |

†-Intermediate calculations

## APPENDIX B

## IN Z Program

This program calculates the input impedance, $Z_{n+1}$, to a length of lossless transmission line with characteristic impedance $Z_o$ and complex load $Z_n = R_n + jX_n$ using the following well known equation

$$Z_{n+1} = Z_o \frac{Z_n + jZ_o \tan \beta \ell}{Z_o + jZ_n \tan \beta \ell} \tag{29}$$

By substituting $Z_n$ into this equation and rationalizing this complex ratio, the solution of $R_{n+1}$ and $X_{n+1}$ may be found. These quantities are as follows,

$$R_{n+1} = \frac{R_n Z_o^2}{D} \tag{30}$$

$$Y_{n+1} = \frac{Z_o[X_n Z_o \cos 2\theta + (Z_o^2 - R_n^2 - X_n^2) \sin\theta \cos\theta]}{D} \tag{31}$$

where $\theta = \beta\ell$ $\qquad D = (Z_o \cos\theta - X_n \sin\theta)^2 + (R_n \sin\theta)^2$

A program listing of this program is provided on page 75. To run the program, it is called from memory and the transmission line length, $\ell$, and frequency are entered in the X and Y stack registers, respectively. The $\mathrm{Re}(Z_{n+1})$ and $\mathrm{Im}(Z_{n+1})$ are stored in storage registers 7 and 8, respectively.

TABLE 6. IN Z Program Listing

| Address | Key | Comment |
|---|---|---|
| 01 | LBL IN Z | |
| 02 | RAD | |
| 03 | * | |
| 04 | PI | |
| 05 | STO + X | |
| 06 | * | |
| 07 | 3 X $10^4$ | |
| 08 | / | |
| 09 | COS | |
| 10 | STO 01 | COS θ |
| 11 | LAST X | |
| 12 | SIN | |
| 13 | STO 02 | SIN θ |
| 14 | RCL 03 | |
| 15 | R↓ | |
| 16 | RCL 04 | |
| 17 | RCL 05 | |
| 18 | R↓ | |
| 19 | X≷Y | |
| 20 | * | |
| 21 | $X^2$ | |
| 22 | RCL 02 | |
| 23 | R↑ | |
| 24 | * | |
| 25 | R↑ | |
| 26 | RCL 03 | |
| 27 | * | |
| 28 | X≷Y | |
| 29 | - | |
| 30 | $X^2$ | |
| 31 | + | |
| 32 | STO 06 | D |
| 33 | RCL 03 | |
| 34 | $X^2$ | |
| 35 | RCL 04 | |
| 36 | * | |
| 37 | X≷Y | |
| 38 | / | |
| 39 | STO 07 | $R_N$ +1 |
| 40 | RCL 03 | |
| 41 | $X^2$ | |
| 42 | RCL 04 | |
| 43 | $X^2$ | |
| 44 | - | |
| 45 | RCL 05 | |
| 46 | $X^2$ | |
| 47 | - | |
| 48 | RCL 01 | |
| 49 | RCL 02 | |
| 50 | * | |
| 51 | * | |
| 52 | RCL 01 | |
| 53 | $X^2$ | |
| 54 | RCL 02 | |
| 55 | $X^2$ | |
| 56 | - | |
| 57 | RCL 03 | |
| 58 | RCL 05 | |
| 59 | * | |
| 60 | * | |
| 61 | + | |
| 62 | RCL 03 | |
| 63 | * | |
| 64 | RCL 06 | |
| 65 | / | |
| 66 | STO 08 | $X_N$+1 |
| 67 | RCL 07 | |
| 68 | X= | |
| 69 | ARCL X | |
| 70 | APPEND Y | |
| 71 | ARCL Y | |
| 72 | AVIEW | |
| 73 | DEG | |
| 74 | RTN | |
| 75 | END | |

## REFERENCES


1. Harp, R.S. and Stover, H.L., Microwave Power Accumulator, U.S. Patent No. 3,931,887, 1971.

2. Kurokawa, K., The Single-Cavity Multiple-Device Oscillator, IEEE MTT Transactions, Vol. 19, No. 10, October 1971,793-801.

3. Harrington, R. F., "Time-Harmonic Electromagnetic Fields," McGraw-Hill Book Company, Inc., New York, 1961.

4. Harp, R.S. and Russell, K.J., Microwave Power Combinatorial Development Task 1: 10 GHz Amplifier Combiner, sponsored by the Air Force Avionics Laboratory, AFAL TR-75-173, November 1975.

5. Russell, K.J., Diode Combining Techniques, sponsored by the Air Force Avionics Laboratory, AFAL TR-79-1108, September 1980.

6. Mastroianni, R.G., Diode Combining Techniques, sponsored by the Air Force Avionics Laboratory, AFAL TR-79-1172, April 1980.

7. Harris, M.J., Ku-Band Amplifier Development, sponsored by the Air Force Avionics Laboratory, AFAL TR-79-1173, November 1979.

8. Ramo, S. and Whinnery, J.R., "Fields and Waves in Modern Radio," John Wiley & Sons, Inc., New York, 1964.

9. Ginzton, E.L., "Microwave Measurements," McGraw-Hill Book Company, Inc., New York, 1957, 391-434.

10. Montgomery, C.G., Dicke, R.H., and Purcell, E.M., "Principles of Microwave Circuits," Radiation Laboratory Series, Vol. 8, McGraw-Hill Book Company, Inc., 1948, 157-239.

11. Altman, J.L., "Microwave Circuits," D. Van Nostrand Co., Inc., New York, 1964, 203-239.

12. Ragan, G.L., "Microwave Transmission Circuits," Radiation Laboratory Series, Vol. 9, McGraw-Hill Book Company, Inc., New York, 1948, 647-709.

13. Marcuvitz, N., "Waveguide Handbook," Radiation Laboratory Series, Vol. 10, McGraw-Hill Book Company, Inc., New York, 1951, 209-216.

14. Montgomery, C.G., "Techniques of Microwave Measurements," Radiation Laboratory Series, Vol. 11, McGraw-Hill Book Company, Inc., New York, 1947, 297-303.

15. Ghose, R.N., "Microwave Circuit Theory & Analysis," McGraw-Hill Book Company, Inc., New York, 1963, Chapter 8.

REFERENCES(con't)

16. Jahnke, E. and Emde F., "Tables of Functions," Dover Publications, Inc., New York, 1945,128-188.

17. "ECCOSORB Data Sheet," Emerson & Cuming, Inc., Canton, Mass.

18. Aston, R., Techniques for Increasing the Bandwidth of a TM010 Mode Power Combiner, IEEE MTT Transactions, Vol. 27, No.5, May 1979, 479-482.

19. Schelkunoff, S.A., "Electomagnetic Waves," Bell Telephone Laboratory Series, D. Van Nostrand Company, Inc., New York, 1943, 267-273.